R. & M. No. 2814
(13,756)
(A.R.C. Technical Report)

MINISTRY OF SUPPLY

AERONAUTICAL RESEARCH COUNCIL
REPORTS AND MEMORANDA

Velocity Distribution on Thin Bodies of Revolution at Zero Incidence in Incompressible Flow

By

S. NEUMARK, Techn.Sc.D., A.F.R.Ae.S.

LONDON: HER MAJESTY'S STATIONERY OFFICE
1954
PRICE 12*s* 6*d* NET

Velocity Distribution on Thin Bodies of Revolution at Zero Incidence in Incompressible Flow

By

S. NEUMARK, Techn.Sc.D., A.F.R.Ae.S.

COMMUNICATED BY THE PRINCIPAL DIRECTOR OF SCIENTIFIC RESEARCH (AIR),
MINISTRY OF SUPPLY

Reports and Memoranda No. 2814*

July, 1950

Summary.—A new method of determining velocity distribution on slender bodies of revolution in axial flow is expounded, analogous to the linear perturbation method widely used for slender symmetrical profiles in two dimensions. The proposed method leads to simple approximate formulae for velocity distribution on a body, once the equation of the meridian line is given, either in the form of a polynomial, or a square root of one. The new method avoids many inconveniences of the older procedures, and is much more rapid. Although theoretically applicable to bodies of small thickness only, it works with satisfactory accuracy up to quite considerable thickness ratios. It has been further improved by taking into account not only axial but also radial velocity components, following a suggestion of Lighthill's supersonic theory. It may be easily applied to compressible subsonic flow.

The method has been used for computing velocity distributions on twelve different bodies, of seven different thickness ratios (0·04–0·28) each, so as to exhibit the most characteristic features in typical cases, and especially to show some unexpected effects of thickness changes. Several practical conclusions have been derived from the examination and comparison of these results.

The method may find useful applications in the design of fuselages, nacelles and wing junctions, and especially in determining critical Mach numbers for such bodies.

1. *Introduction.*—Axial potential flow past bodies of revolution has been the subject of several rigorous investigations in theoretical hydrodynamics, and much of this work has been summarized in Chapter V of Lamb's Hydrodynamics[1]. The existing rigorous solutions are not numerous and apply rather to some particular geometrical shapes, while it is very difficult to find such solutions, giving velocity potential and velocity distributions for arbitrarily chosen meridian lines. The inverse problem, *i.e.*, designing meridian lines for assumed velocity distributions, is even less tractable on the lines of the exact theory. Hence, there have been several attempts to work out simpler methods applicable to elongated bodies suitable for airships or aircraft fuselages and nacelles. These methods usually followed Rankine's idea of distributing point sources and sinks along the axis (Ref. 1, Art. 97). Systems of isolated sources and semi-continuous or continuous source distributions were all tried[2,3,4], and shapes of more or less the required form could be obtained, and the velocities calculated, in a rather cumbrous way. An extremely elaborate method, based on sources and sinks in special curvilinear co-ordinates, with rigorous solutions by infinite series for arbitrarily assumed shapes, was worked out by Kaplan[5]. This is highly accurate but so troublesome to apply that it may be only seldom used, *e.g.*, as a dependable check for simpler approximate methods.

* R.A.E. Report Aero. 2389, received 3rd February, 1951.

For the analogous two-dimensional problem of symmetrical profiles at zero incidence, though admitting a comparatively easy solution by conformal transformation, a strikingly simple approximate method has been introduced by Squire[6] and others. This applies to profiles of small thickness ratio ϑ and is based on continuous distribution of (linear) sources and sinks along the chord, with three simplifying assumptions: (a) the local strength of the source distribution is taken to be proportional to the local slope of the profile contour; (b) the velocity component v_x parallel to the chord, induced by the source system, is calculated not along the contour but along the chord; (c) the component v_z perpendicular to the chord is neglected. The procedure gives finite values, small of the order ϑ, of the induced velocities everywhere, except at stagnation points, and it is easily proved that errors are small of the order ϑ^2. This method is a particular case of the much more general ' linear perturbation theory ', as worked out by Goldstein and Young (R. & M. 1909[7]). It has found application also in three-dimensional problems, expecially for swept-back wings at zero incidence (R. & M. 2713[11]).

An idea suggests itself, to try a similar method for thin bodies of revolution, the local strength of source distribution along the axis having to be assumed this time as proportional to the local rate of increase of the cross-section area. However, one fundamental difficulty arises, in that the axial velocity component v_x, induced by such a source system, becomes logarithmically infinite on the axis itself. This makes it impossible to introduce the simplifying assumption (b) as above. Young and Owen tried to overcome this difficulty by calculating v_x, instead of on the given surface, on that of an ellipsoid of revolution of the same length and thickness ratio, and this led to their simplified theory (R. & M. 2071[8]), as applied to development of high-speed or low-drag shapes (R. & M. 2204[10]). This theory is neither a true analogue of the two-dimensional linear method, nor so simple as that one (though much simpler than Kaplan's solution); it leaves some doubts as to the order of magnitude of v_x and of the errors involved, and also as to the effect of varying thickness ratio. Its merit is that it can be worked both for the direct and the inverse problem.

It is shown in this report that the difficulty mentioned above can be overcome in quite a different way. The integral for v_x, which becomes logarithmically infinite on the axis, may be transformed so that only one simple term infinite on the axis remains, while the rest of the integral may be calculated on the axis, with all resulting simplifications. It appears that the total v_x induced consists of two terms, one being small of the order $\vartheta^2 \ln \vartheta$ and the other one of the order ϑ^2. Both must be taken into account, and the errors committed are of the order $\vartheta^4 \ln \vartheta$, ϑ^4, and higher. One important conclusion is that the velocity distribution varies with ϑ not in proportion to any function of ϑ, and that indeed the law of distribution itself may be modified considerably owing to a change in thickness ratio so that, *e.g.*, the position of maximum supervelocity may be shifted, or even the number of maxima altered. This is very different from what happens in two dimensions where supervelocities are simply proportional to ϑ, in first approximation. The inference bears upon the effects of compressibility (*see* R. & M. 2624[12] and Ref. 14). The comparison of the new method with that of Young and Owen shows that the latter is not free from errors of the order ϑ^2.

The analytical procedure suggested leads to an entirely new method of calculation (section 2) reposing on the formula (2.24) for v_x. It is further improved (following Lighthill's (R. & M. 2003[9]) suggestion in connection with supersonic theory) by introducing the radial component v_r; this, being itself small of the order ϑ, involves a contribution of the order ϑ^2 to the resultant supervelocity (formulae 2.27 and 2.29). The method is particularly suitable when the meridian line is expressed by an algebraic equation, especially in the form of a polynomial, or a square root of a polynomial (so that the square of the ordinate is, in both cases, expressed by a polynomial in terms of the abscissa). Such an equation suffices to cover practically all shapes likely to be of interest, including those with rounded, pointed, and cusped noses and tail ends. Explicit formulae, involving a large number of arbitrary coefficients, and specified for particular classes of bodies, are given in section 3. This is followed by a number of examples in section 4,

illustrated by Figs. 3 to 15, including some characteristic geometrical shapes and some suitable for fuselages and nacelles. Velocity diagrams have been computed, showing the contributions of v_x and v_r separately and the resultant supervelocity ratio $\Delta V/U$, for seven different thickness ratios (0·04–0·28) in each case. The results are discussed, leading to several practical conclusions, in section 5. An Appendix deals with the question of inaccuracies caused by larger thickness ratio, by comparing exact and approximate solutions for ellipsoids of revolution.

The new method is not directly applicable for solving the inverse problem, *i.e.*, designing shapes for assumed velocity distributions. This, however, should lose some of its importance, for the following reasons. First of all, the new method is so rapid and simple that a great number of shapes may be examined easily with little outlay of time and effort; and then shapes may be chosen to suit any *realizable* velocity distributions. Further, the designer has to adapt the shape to so many constructional and technological requirements, that the main question for him is to find out whether an otherwise convenient shape will have a reasonably advantageous velocity distribution, and what changes are needed to improve this distribution if necessary. For such purposes, the proposed method should be particularly suited.

Acknowledgements are due to R. P. Purkiss and A. R. Beauchamp for their help in computational work and in preparing the illustrations.

2. *Fundamentals of the Method.*—Let us consider an arbitrary body of revolution (Fig. 1), the equation of whose meridian line is:

$$r = r(x) \qquad (-b < x < b) \qquad (2.1)$$

It will be convenient to introduce the function:

$$F(x) = r^2 , \qquad (2.2)$$

so that the area A of a cross-section at a station x will be:

$$A = \pi \, . \, F(x) \, . \qquad (2.3)$$

The first derivative of (2.2) is:

$$F'(x) = 2r \, . \, r'(x) \, . \qquad (2.4)$$

Suppose now that the body is thin, *i.e.*, that its thickness ratio:

$$\vartheta = r_{\max}/b \qquad (2.5)$$

may be considered as small. Then $r(x)$ and its derivatives are small of the order ϑ, while $F(x)$ and its derivatives are small of the order ϑ^2.

We consider the flow of an ideal incompressible fluid, with undisturbed velocity U parallel to the x axis and directed against it. In order to determine the velocity distribution on the body surface, we assume tentatively that the disturbance due to the presence of the body is equivalent to that produced by a continuous distribution of sources and sinks along the axis. Denoting by $q(\bar{x})$ the local source intensity (per unit length) at a station $\bar{x}$, where the area is $\bar{A}$, we may write, as a first order approximation:

$$q(\bar{x}) = - U \frac{d\bar{A}}{d\bar{x}} = - \pi \, . \, U \, . \, F'(\bar{x}) \qquad (-b < \bar{x} < b) \ldots \qquad (2.6)$$

This formula is based on the assumption that the resultant velocity of the flow, both outside and inside the body, differs little from U in direction and magnitude. The flux across any cross-section is then approximately $U\bar{A}$, and its infinitesimal increment $Ud\bar{A}$ must be supplied by the output $qd\bar{x}$ of the infinitesimal segment $d\bar{x}$ of the source line.

We shall determine the two components v_r and v_x of the velocity induced by the source line at a point (x, r) of the body surface. An infinitesimal element of length $d\bar{x}$ induces a velocity:

$$\delta v = \frac{q(\alpha) \, . \, d\bar{x}}{4\pi R^2} = - \frac{U}{4} \, . \, \frac{F'(\bar{x}) \, . \, d\bar{x}}{R^2} \, , \qquad (2.7)$$

where

$$R^2 = (\bar{x} - x)^2 + r^2 . \qquad (2.8)$$

The r- and x-components of δv are:

$$dv_r = \cos\theta \, . \, \delta v = -\frac{U}{4} \cdot \frac{rF'(\bar{x}) \, . \, d\bar{x}}{R^3} , \qquad (2.9)$$

$$dv_x = -\sin\theta \, . \, \delta v = \frac{U}{4} \frac{(\bar{x} - x) \, . \, F'(\bar{x}) \, . \, d\bar{x}}{R^3} , \qquad (2.10)$$

and the integral components:

$$v_r = -\frac{U}{4} \int_{-b}^{b} \frac{r \, . \, F'(\bar{x}) \, . \, d\bar{x}}{\{(\bar{x} - x)^2 + r^2\}^{3/2}} , \qquad (2.11)$$

$$v_x = \frac{U}{4} \int_{-b}^{b} \frac{(\bar{x} - x) \, . \, F'(\bar{x}) \, . \, d\bar{x}}{\{(\bar{x} - x)^2 + r^2\}^{3/2}} . \qquad (2.12)$$

Let us introduce an auxiliary variable:

$$p = \bar{x} - x \quad (\text{thus } dp = d\bar{x}) , \qquad (2.13)$$

and a sequence of definite integrals:

$$I_k = \int_{-(b+x)}^{b-x} \frac{p^k dp}{(p^2 + r^2)^{3/2}} \qquad (k = 0, 1, 2, 3, \ldots) . \qquad (2.14)$$

By applying the theorem of mean value, and taking into account (2.4), the formula (2.11) may be written:

$$\frac{v_r}{U} = -\tfrac{1}{4} \int_{-(b+x)}^{b-x} \frac{rF'(x + p) \, . \, dp}{(p^2 + r^2)^{3/2}} = -\tfrac{1}{2} r'(x) \, . \, r^2 I_0 - \tfrac{1}{4} rK \, . \, I_1 , \qquad (2.15)$$

where K denotes a certain mean value of $F''(x)$, smaller than the upper bound of $|F''(x)|$ if such a bound exists.

To transform (2.12), we shall write, by Taylor's expansion:

$$F'(\bar{x}) = F'(x + p) = F'(x) + pF''(x) + \sum_{k=1} \frac{p^{k+1}}{(k+1)!} F^{k+2}(x) , \qquad (2.16)$$

the Σ denoting a finite sum if $F(x)$ is a polynomial, or an infinite series in all other cases. Substituting (2.13) and (2.16) into (2.12), we obtain:

$$\frac{v_x}{U} = \tfrac{1}{4} F'(x) \, . \, I_1 + \tfrac{1}{4} F''(x) \, . \, I_2 + \tfrac{1}{4} \sum_{k=1} \frac{F^{k+2}(x)}{(k+1)!} I_{k+2} . \qquad (2.17)$$

We now need explicit formulae for the integrals (2.14). The first three of them are easily found as follows:

$$\int \frac{dp}{(p^2 + r^2)^{3/2}} = \frac{p}{r^2(p^2 + r^2)^{1/2}} , \text{ hence } r^2 I_0 = \frac{b - x}{((b - x)^2 + r^2)^{1/2}} + \frac{b + x}{((b + x)^2 + r^2)^{1/2}} , \qquad (2.18_0)$$

$$\int \frac{p dp}{(p^2 + r^2)^{3/2}} = -\frac{1}{(p^2 + r^2)^{1/2}} , \text{ hence } I_1 = \frac{1}{((b + x)^2 + r^2)^{1/2}} - \frac{1}{((b - x)^2 + r^2)^{1/2}} , \qquad (2.18_1)$$

$$\int \frac{p^2 dp}{(p^2 + r^2)^{3/2}} = -\frac{p}{(p^2 + r^2)^{1/2}} + \ln\,(p + (p^2 + r^2)^{1/2}) ,$$

$$\text{hence} \qquad I_2 = -r^2 I_0 + \ln \frac{((b - x)^2 + r^2)^{1/2} + (b - x)}{((b + x)^2 + r^2)^{1/2} - (b + x)} , \qquad (2.18_2)$$

or, expanding in powers of r^2:

$$r^2 I_0 = 2 - \frac{r^2(b^2 + x^2)}{(b^2 - x^2)^2} \cdots \qquad (2.19_0)$$

$$I_1 = -\frac{2x}{b^2 - x^2} + \frac{r^2 x(3b^2 + x^2)}{(b^2 - x^2)^3} \cdots \qquad (2.19_1)$$

$$I_2 = 2\left(\ln \frac{2(b^2 - x^2)^{1/2}}{r} - 1\right) + \frac{3}{2}\frac{r^2(b^2 + x^2)}{(b^2 - x^2)^2} \cdot \qquad (2.19_2)$$

All subsequent integrals I_{k+2}, for $k \geqslant 1$, may be obtained by applying the obvious recurrence formula:

$$\int \frac{p^{k+2}\,dp}{(p^2 + r^2)^{3/2}} = \frac{p^{k+1}}{k(p^2 + r^2)^{1/2}} - \frac{k+1}{k} r^2 \int \frac{p^k\,dp}{(p^2 + r^2)^{3/2}}, \qquad (2.20)$$

whence:

$$I_{k+2} = \frac{1}{k}\left\{\frac{(b - x)^{k+1}}{((b - x)^2 + r^2)^{1/2}} - \frac{(-b - x)^{k+1}}{((b + x)^2 + r^2)^{1/2}}\right\} - \frac{k+1}{k} r^2 I_k, \qquad (2.21)$$

or expanding again:

$$I_{k+2} = \frac{(b - x)^k + (-b - x)^k}{k} - \frac{r^2}{2k}\left[(b - x)^{k-2} + (-b - x)^{k-2} + 2(k+1) I_k\right]. \qquad (2.22)$$

Let us consider (2.15). The product $r^2 I_0$ tending to 2 with decreasing r, the first term is small of the order ϑ, while the second one is small of the order ϑ^3. Therefore, neglecting small terms of the order ϑ^3 and higher, we obtain:

$$v_r/U = -r'(x), \qquad (2.23)$$

and this shows that the boundary conditions on the body surface are satisfied, to this order of accuracy.

The component v_x on the surface should now be calculated from (2.17). This would be long and troublesome, if exact values of the integrals I_1, I_2, etc., were to be computed; also, the accuracy would be illusory, as the boundary conditions are only approximately satisfied. In the two-dimensional problem, v_x is simply calculated on the x axis instead of on the wing surface, and it is shown that the error thus committed is small of the 2nd order. A similar simplification may be attempted in our problem, which means that the exact values of the integrals I_1, I_2, etc., would be replaced by their respective values on the x axis (putting $r = 0$). It is seen that this can be done with all integrals *except* I_2, the latter becoming logarithmically infinite* for $r = 0$, as shown by (2.19$_2$). Even I_2, however, may be simplified, by rejecting in (2.19$_2$) all terms except the first one. Introducing the simplified expressions for all integrals in (2.17), we obtain:

$$\frac{v_x}{U} = \tfrac{1}{2}F''(x) \cdot \ln \frac{2(b^2 - x^2)^{1/2}}{r} - \frac{1}{2}\left[\frac{xF'(x)}{b^2 - x^2} + F''(x) - \sum_{k=1} \frac{F^{k+2}(x)}{(k+1)!} \frac{(b - x)^k + (-b - x)^k}{2k}\right]. \qquad (2.24)$$

The first term is small of the order $\vartheta^2 \ln \vartheta$, all subsequent ones small of the order ϑ^2. The neglected terms are small of the order $\vartheta^4 \ln \vartheta$, or ϑ^4, or higher.

* It is due to this term only that the total v_x becomes infinite on the axis.

The formula (2.24) is suggested as a simple means of calculating v_x, especially if $F(x)$ is a finite polynomial of any degree, because then the second term (in square bracket) becomes a simple algebraic function. This may be considered to cover all meridian line shapes which have a practical meaning, as every such shape can be represented by a polynomial $F(x)$ with a great accuracy, whether the nose or tail end are rounded, pointed or cusped. Section 3 contains explicit formulae for several fundamental classes of meridian lines, and Section 4 a number of particular examples.

The formula (2.24) is a counterpart of similar (simpler) formulae relating to two-dimensional symmetrical wing profiles (*see, e.g.*, R. & M. 2713[11], form. I.8 and I.14). The main difference is as follows. The two-dimensional formula contains only terms of 1st order in thickness ratio ϑ, and therefore the incremental velocities are simply proportional to ϑ. One computation is sufficient for all thickness ratios, the supervelocity diagrams for varying ϑ are similar curves, and hence, for instance, the position of maximum supervelocity is independent of ϑ. In the present case, the formula contains one term of the order $\vartheta^2 \ln \vartheta$, and others of the order ϑ^2. There is only an infinitesimal difference between two orders of smallness, and clearly terms of both orders must be kept, but v_x is not simply proportional to ϑ^2 and must be calculated separately for each thickness ratio. The diagrams will not be similar curves, and the position of maximum supervelocity will depend on ϑ.

It is also seen that the supervelocities on a body of revolution are generally smaller than those on a profile of the same thickness ratio in two-dimensional flow. However, they are not negligible except for very low thickness ratios.

In two dimensions, both supervelocity components v_x and v_z are small of the same order (ϑ); hence the resultant velocity:

$$\left((-U + v_x)^2 + {v_z}^2\right)^{1/2}$$

may be taken as $(-U + v_x)$, accurate to the order ϑ, and the contribution of v_z may be neglected. It has been pointed out by Lighthill (R. & M. 2003[9]), with reference to supersonic flow, that the contribution of v_r must not be neglected in the case of bodies of revolution, and this applies also in our present problem. The resultant velocity is (Fig. 2):

$$V = \left((-U + v_x)^2 + {v_r}^2\right)^{1/2} = U\left(1 - 2\frac{v_x}{U} + \frac{{v_x}^2}{U^2} + \frac{{v_r}^2}{U^2}\right)^{1/2}, \quad \ldots \quad \ldots \quad (2.25)$$

and it is seen that the second and fourth terms under the root sign are small of comparable order ($\vartheta^2 \ln \vartheta$ and ϑ^2, respectively), while the third one is small of higher order ($\vartheta^4 \ln^2 \vartheta$) and can be neglected. We then get, to the order of $\vartheta^2 \ln \vartheta$ and ϑ^2:

$$V = U\left(1 - \frac{v_x}{U} + \frac{{v_r}^2}{2U^2}\right), \quad \ldots \quad \ldots \quad \ldots \quad \ldots \quad \ldots \quad \ldots \quad \ldots \quad (2.26)$$

whence:

$$\frac{\Delta V}{U} = \frac{V - U}{U} = -\frac{v_x}{U} + \frac{{v_r}^2}{2U^2}, \quad \ldots \quad \ldots \quad \ldots \quad \ldots \quad \ldots \quad \ldots \quad \ldots \quad (2.27)$$

and ΔV will be called the approximate resultant supervelocity. The first term in (2.27) is normally more important, but the second one may influence the result in a not inconsiderable way, as will be shown in the examples. It will be convenient to represent this second term as follows. From (2.23):

$$\frac{{v_r}^2}{2U^2} = \tfrac{1}{2}\left\{r'(x)\right\}^2, \quad \ldots \quad \ldots \quad \ldots \quad \ldots \quad \ldots \quad \ldots \quad \ldots \quad \ldots \quad (2.28)$$

and, taking into account (2.2) and 2.4):

$$\frac{v_r^2}{2U^2} = \frac{\{F'(x)\}^2}{8F(x)} \quad \ldots \quad (2.29)$$

The final conclusion is that the supervelocity ratio $\Delta V/U$ must be calculated from (2.27), where the first term is supplied by (2.24) and the second one by (2.29).

It is interesting to compare the new method with that of Young and Owen (R. & M. 2071[8]). Their procedure was based on the same system of sources and sinks but, to avoid the infinite values on the axis, they calculated v_x on the surface of the ellipsoid or revolution:

$$r_{el} = \vartheta(b^2 - x^2)^{1/2}$$

of the same thickness ratio as the given body. They assumed that the error thus committed would be small. It will be seen by inspecting our formulae (2.17-2.24) that the errors in most terms are of higher orders and negligible (as in our method), but the first term in (2.24) is exceptional. Replacing the true r by r_{el} in this term means an error:

$$\tfrac{1}{2}F''(x) \,.\, \ln r/r_{el} \,,$$

which is of the order ϑ^2, thus not negligible. For an ellipsoid, $F''(x)$ is a constant, equal to $(-2\vartheta^2)$. Even supposing that, for any other body, $F''(x)$ does not exceed this value (which it often may), we should estimate the error as

$$\vartheta^2 \ln r/r_{el} \,.$$

This may be very small when the body differs little from an ellipsoid, but may become significant in other cases. For instance, if the ratio r/r_{el} reaches the value 2 at any point in the meridian line, the error there may become $0{\cdot}69\vartheta^2$, or perhaps more. The errors are often smaller than this, of course, and most results of R. & M. 2071[8], especially the maximum values of supervelocities, do not deviate appreciably. The present method, however, seems to ensure better accuracy, is more rapid, and gives explicit formulae in each case, as will be shown in the following sections.

3. *Detailed Formulae for Particular Classes of Bodies of Revolution.*—3.1. *General (bodies with rounded nose and tail end, e.g., Figs.* 3, 10, 13).—Assuming that $F(x)$ is a polynomial of the 8th degree or lower, and introducing non-dimensional co-ordinates:

$$\xi = x/b \,, \qquad \rho = r/b \,, \quad \ldots \quad (3.1.1)$$

we may write the equation of the meridian line as follows:

$$\rho = k\vartheta(A_0 + A_1\xi + A_2\xi^2 + \ldots + A_8\xi^8)^{1/2} \,, \quad \ldots \quad (3.1.2)$$

where:

$$k = \frac{1}{(A_0 + A_1 m + A_2 m^2 + \ldots + A_8 m^8)^{1/2}} \,, \quad \ldots \quad (3.1.3)$$

m denoting the value of ξ, between (-1) and $(+1)$, at which ρ reaches its maximum. The function $F(x)$ then becomes:

$$F(x) = k^2\vartheta^2 b^2 \sum_{n=0}^{8} A_n \xi^n \,, \quad \ldots \quad (3.1.4)$$

and we obtain from (2.24), after an elementary but long transformation:

$$\frac{v_x}{Uk^2\vartheta^2} = \ln \frac{2(1-\xi^2)^{1/2}}{\rho} \cdot \sum_{2}^{8} \frac{n(n-1)}{2} A_n \xi^{n-2} + \frac{1}{1-\xi^2} \cdot \sum_{0}^{8} K_n \xi^n \,, \quad \ldots \quad (3.1.5)$$

where the coefficients K_n are given by the following table:

n	K_n								
0		$-A_2$		$+A_4$		$+\frac{3}{4}A_6$			$+\frac{2}{3}A_8$
1	$-\frac{1}{2}A_1$		$-\frac{9}{2}A_3$		$+\frac{5}{2}A_5$		$+\frac{7}{4}A_7$		
2				$-12A_4$		$+\frac{15}{4}A_6$			$+\frac{7}{5}A_8$
3			$3A_3$		$-\frac{70}{3}A_5$		$+\frac{21}{4}A_7$		
4				$9A_4$		$-\frac{155}{4}A_6$			$+7A_8$
5					$\frac{55}{3}A_5$		$-\frac{1169}{20}A_7$		
6						$\frac{125}{4}A_6$			$-\frac{413}{5}A_8$
7							$\frac{959}{20}A_7$		
8									$\frac{343}{5}A_8$

The contribution of the v_r component, after (2.29), becomes:

$$\frac{v_r^2}{2U^2k^2\vartheta^2} = \left(\sum_1^8 nA_n\xi^{n-1}\right)^2 : 8\sum_0^8 A_n\xi^n . \qquad (3.1.6)$$

The above results may be represented in a more convenient form. The function $F(x)$ must become 0 at the nose and at the tail end, and hence it must contain $(1-\xi)$ and $(1+\xi)$ as factors. If both occur only once as factors of $F(x)$, the body has a *rounded nose and rounded tail end.* We may then write:

$$\rho = k\vartheta\{(1-\xi^2)(B_0 + B_1\xi + B_2\xi^2 + B_3\xi^3 + B_4\xi^4 + B_5\xi^5 + B_6\xi^6)\}^{1/2}, \qquad (3.1.7)$$

and

$$F(x) = k^2\vartheta^2b^2(1-\xi^2)\cdot\sum_0^6 B_n\xi^n . \qquad (3.1.8)$$

We have then:

$$\left.\begin{aligned} A_0 = B_0,\ A_1 = B_1,\ A_2 = B_2 - B_0,\ A_3 = B_3 - B_1,\ A_4 = B_4 - B_2,\\ A_5 = B_5 - B_3,\ A_6 = B_6 - B_4,\ A_7 = -B_5,\ A_8 = -B_6, \end{aligned}\right\} \qquad (3.1.9)$$

and, substituting this in (3.1.5) and (3.1.6), we obtain:

$$-\frac{v_x}{Uk^2\vartheta^2} = \ln\frac{(1-\xi^2)^{1/2}}{\rho}\cdot\sum_{n=0}^6 P_n\xi^n - \frac{1}{1-\xi^2}\cdot\sum_0^8 K_n\xi^n, \qquad (3.1.10)$$

$$\frac{v_r^2}{2U^2k^2\vartheta^2} = \left(\sum_0^7 R_n\xi^n\right)^2 : 8(1-\xi^2)\cdot\sum_0^6 B_n\xi^n , \qquad (3.1.11)$$

the coefficients K_n, P_n, R_n being tabulated below:

n	K_n					P_n	R_n
0	B_0	$-2B_2$		$+\frac{1}{4}B_4$	$+\frac{1}{12}B_6$	$B_0 - B_2$	B_1
1	$4B_1$		$-7B_3$		$+\frac{3}{4}B_5$	$3(B_1 - B_3)$	$2(B_2 - B_0)$
2		$12B_2$		$-\frac{63}{4}B_4$	$+\frac{171}{2}B_6$	$6(B_2 - B_4)$	$3(B_3 - B_1)$
3	$-3B_1$		$+\frac{79}{3}B_3$		$-\frac{343}{12}B_5$	$10(B_3 - B_5)$	$4(B_4 - B_2)$
4		$-9B_2$		$+\frac{1911}{4}B_4$	$-\frac{1883}{4}B_6$	$15(B_4 - B_6)$	$5(B_5 - B_3)$
5			$-\frac{55}{3}B_3$		$+\frac{46607}{60}B_5$	$21B_5$	$6(B_6 - B_4)$
6				$-\frac{125}{4}B_4$	$+\frac{22771}{20}B_6$	$28B_6$	$-7B_5$
7					$-\frac{959}{20}B_5$	—	$-8B_6$
8					$-\frac{343}{5}B_6$	—	—

These results are quite general and may be always used, but they are really convenient only if both the nose and the tail end are rounded. If either of them is pointed or cusped, one of the binomials $(1 - \xi)$ or $(1 + \xi)$ occurs twice, three times, etc., as a factor of $F(x)$. The formulae may then be simplified, and the simpler results are given below for all cases which are likely to have a practical meaning.

3.2. *Bodies with Rounded Nose and Pointed Tail End* (*e.g.*, Figs. 7, 8, 12, 14).—The equation of the meridian line:

$$\rho = k\vartheta(1 + \xi)\{(1 - \xi)(D_0 + D_1\xi + D_2\xi^2 + D_3\xi^3 + D_4\xi^4 + D_5\xi^5)\}^{1/2}, \quad .. \quad (3.2.1)$$

and

$$F(x) = k^2\vartheta^2b^2(1 + \xi)^2(1 - \xi) \cdot \sum_0^5 D_n\xi^n \, . \quad .. \quad .. \quad .. \quad .. \quad .. \quad (3.2.2)$$

The contributions of the axial and radial supervelocity components are given by:

$$-\frac{v_x}{Uk^2\vartheta^2} = \ln\frac{2(1 - \xi^2)^{1/2}}{\rho} \cdot \sum_0^6 P_n\xi^n - \frac{1}{1 - \xi}\sum_0^7 K_n'\xi^n, \quad .. \quad .. \quad .. \quad .. \quad (3.2.3)$$

$$\frac{v_r^2}{2U^2k^2\vartheta^2} = \Big(\sum_0^6 S_n\xi^n\Big)^2 : 8(1 - \xi) \cdot \sum_0^5 D_n\xi^n, \quad .. \quad .. \quad .. \quad .. \quad .. \quad (3.2.4)$$

the coefficients being as follows:

n	K_n'					P_n	S_n
0	D_0	$-2D_1$	$-2D_2$	$+\frac{1}{4}D_3$	$+\frac{1}{4}D_4$ $+\frac{1}{12}D_5$	$D_0 - D_1 - D_2$	$D_0 + D_1$
1	$3D_0$	$+6D_1$	$-5D_2$	$-\frac{29}{4}D_3$	$+\frac{1}{2}D_4$ $+\frac{2}{3}D_5$	$3(D_0 + D_1 - D_2 - D_3)$	$-3D_0 + D_1 + 2D_2$
2	$-3D_0$	$+6D_1$	$+17D_2$	$-\frac{17}{2}D_3$	$-\frac{65}{4}D_4$ $+\frac{3}{4}D_5$	$6(D_1 + D_2 - D_3 - D_4)$	$-4D_1 + D_2 + 3D_3$
3		$-9D_1$	$+\frac{28}{3}D_2$	$+\frac{209}{6}D_3$	$-\frac{37}{3}D_4$ $-\frac{88}{3}D_5$	$10(D_2 + D_3 - D_4 - D_5)$	$-5D_2 + D_3 + 4D_4$
4			$-\frac{55}{3}D_2$	$+\frac{1555}{12}D_3$	$+\frac{721}{12}D_4$ $-\frac{197}{12}D_5$	$15(D_3 + D_4 - D_5)$	$-6D_3 + D_4 + 5D_5$
5				$-\frac{125}{4}D_3$	$+\frac{167}{10}D_4$ $+\frac{466}{5}D_5$	$21(D_4 + D_5)$	$-7D_4 + D_5$
6					$-\frac{959}{20}D_4$ $+\frac{413}{20}D_5$	$28D_5$	$-8D_5$
7					$-\frac{343}{5}D_5$	—	—

3.3. *Bodies with Pointed Nose and Tail End* (*e.g.*, *Figs.* 4, 11).—

$$\rho = k\vartheta(1-\xi^2)(E_0 + E_1\xi + E_2\xi^2 + E_3\xi^3 + E_4\xi^4)^{1/2} \quad .. \quad .. \quad .. \quad .. \quad (3.3.1)$$

$$F(x) = k^2\vartheta^2 b^2(1-\xi^2)^2 \cdot \sum_0^4 E_n\xi^n \quad .. \quad .. \quad .. \quad .. \quad .. \quad .. \quad .. \quad (3.3.2)$$

$$-\frac{v_x}{Uk^2\vartheta^2} = \ln\frac{2(1-\xi^2)^{1/2}}{\rho} \cdot \sum_0^6 P_n\xi^n - \sum_0^6 K_n''\xi^n \quad .. \quad .. \quad .. \quad .. \quad .. \quad (3.3.3)$$

$$\frac{v_r^2}{2U^2k^2\vartheta^2} = \left(\sum_0^5 S_n'\xi^n\right)^2 : 8\sum_0^4 E_n\xi^n \quad .. \quad .. \quad .. \quad .. \quad .. \quad .. \quad .. \quad (3.3.4)$$

n	K_n''	P_n	S_n'
0	$3E_0 \quad -\frac{9}{4}E_2 \quad +\frac{1}{6}E_4$	$2E_0-E_2$	E_1
1	$11E_1 \quad -\frac{31}{4}E_3$	$3(2E_1-E_3)$	$-4E_0 \quad +2E_2$
2	$-9E_0 \quad +\frac{51}{2}E_2 \quad -17E_4$	$-6(E_0-2E_2+E_4)$	$-5E_1 \quad +3E_3$
3	$-\frac{55}{3}E_1 \quad +\frac{283}{6}E_3$	$-10(E_1-2E_3)$	$-6E_2 \quad +4E_4$
4	$-\frac{125}{4}E_2 \quad +\frac{153}{2}E_4$	$-15(E_2-2E_4)$	$-7E_3$
5	$-\frac{959}{20}E_3$	$-21E_3$	$-8E_4$
6	$-\frac{343}{5}E_4$	$-28E_4$	—

3.4. *Bodies with Rounded Nose and Cusped Tail End* (*e.g.*, *Fig.* 9).—

$$\rho = k\vartheta(1+\xi)\{(1-\xi^2)(H_0 + H_1\xi + H_2\xi^2 + H_3\xi^3 + H_4\xi^4)\}^{1/2} \quad .. \quad .. \quad (3.4.1)$$

$$F(x) = k^2\vartheta^2 b^2(1+\xi)^3(1-\xi) \cdot \sum_0^4 H_n\xi^n \quad .. \quad .. \quad .. \quad .. \quad .. \quad .. \quad (3.4.2)$$

$$-\frac{v_x}{Uk^2\vartheta^2} = \ln\frac{2(1-\xi^2)^{1/2}}{\rho} \cdot (1+\xi) \cdot \sum_0^5 P_n'\xi^n - \frac{1}{1-\xi}\sum_0^7 K_n'\xi^n \quad .. \quad .. \quad .. \quad (3.4.3)$$

$$\frac{v_r^2}{2U^2k^2\vartheta^2} = (1+\xi) \cdot \left(\sum_0^5 T_n\xi^n\right)^2 : 8(1-\xi)\sum_0^4 H_n\xi^n \quad .. \quad .. \quad .. \quad .. \quad (3.4.4)$$

n	K_n'	P_n'	T_n
0	$-H_0 \quad -4H_1 \quad -\frac{7}{4}H_2 \quad +\frac{1}{2}H_3 \quad +\frac{1}{3}H_4$	$-2H_1-H_2$	$2H_0+H_1$
1	$9H_0 \quad +H_1 \quad -\frac{49}{4}H_2 \quad -\frac{27}{4}H_3 \quad +\frac{7}{6}H_4$	$6H_0+2H_1-5H_2-3H_3$	$-4H_0+2H_1+2H_2$
2	$3H_0 \quad +23H_1 \quad +\frac{17}{2}H_2 \quad -\frac{99}{4}H_3 \quad -\frac{31}{2}H_4$	$10H_1+5H_2-9H_3 \quad -6H_4$	$-5H_1+2H_2+3H_3$
3	$-9H_0 \quad +\frac{1}{3}H_1 \quad +\frac{265}{6}H_2 \quad +\frac{45}{2}H_3 \quad -\frac{125}{3}H_4$	$15H_2+9H_3-14H_4$	$-6H_2+2H_3+4H_4$
4	$-\frac{55}{3}H_1 \quad -\frac{65}{12}H_2 \quad +73H_3 \quad +\frac{131}{3}H_4$	$21H_3+14H_4$	$-7H_3+2H_4$
5	$-\frac{125}{4}H_2 \quad -\frac{291}{20}H_3 \quad +\frac{1099}{10}H_4$	$28H_4$	$-8H_4$
6	$-\frac{959}{20}H_3 \quad -\frac{273}{10}H_4$	—	—
7	$-\frac{343}{5}H_4$	—	—

3.5. *Bodies with Pointed Nose and Cusped Tail End.*—

$$\rho = k\vartheta(1-\xi^2)\{(1+\xi)(L_0+L_1\xi+L_2\xi^2+L_3\xi^3)\}^{1/2} \quad .. \quad .. \quad .. \quad .. \quad (3.5.1)$$

$$F(x) = k^2\vartheta^2b^2(1-\xi)^2(1+\xi)^3 \cdot \sum_0^3 L_n\xi^n \quad .. \quad .. \quad .. \quad .. \quad .. \quad .. \quad (3.5.2)$$

$$-\frac{v_x}{Uk^2\vartheta^2} = \ln\frac{2(1-\xi^2)^{1/2}}{\rho} \cdot (1+\xi)\sum_0^5 P_n'\xi^n - \sum_0^6 K_n''\xi^n \quad .. \quad .. \quad .. \quad .. \quad (3.5.3)$$

$$\frac{v_r^2}{2U^2k^2\vartheta^2} = (1+\xi)\cdot\left(\sum_0^4 S_n''\xi^n\right)^2 : 8\sum_0^3 L_n\xi^n \quad .. \quad .. \quad .. \quad .. \quad .. \quad (3.5.4)$$

n	K_n''	P_n'	S_n''
0	$3L_0 \quad -\frac{9}{4}(L_1+L_2) \quad +\frac{1}{6}L_3$	$2L_0 \ -L_1 \ -L_2$	L_0+L_1
1	$11(L_0+L_1) \quad -\frac{31}{4}(L_2+L_3)$	$4L_0 \ +7L_1 \ -2L_2 \ -3L_3$	$-5L_0 \ +L_1+2L_2$
2	$-9L_0 \quad +\frac{51}{2}(L_1+L_2) \quad -17L_3$	$-10L_0 \ +5L_1+14L_2 \ -3L_3$	$-6L_1 \ +L_2+3L_3$
3	$-\frac{55}{3}(L_0+L_1) \quad +\frac{283}{6}(L_2+L_3)$	$-15L_1 \ +6L_2+23L_3$	$-7L_2+ \ L_3$
4	$-\frac{125}{4}(L_1+L_2) \quad +\frac{153}{2}L_3$	$-21L_2 \ +7L_3$	$-8L_3$
5	$-\frac{359}{20}(L_2+L_3)$	$-28L_3$	—
6	$-\frac{343}{5}L_3$	—	—

3.6. *Bodies with Cusped Nose and Tail End* (*e.g.*, *Figs.* 5, 6).—

$$\rho = k\vartheta(1-\xi^2)\{(1-\xi^2)(M_0+M_1\xi+M_2\xi^2)\}^{1/2} \quad .. \quad .. \quad .. \quad .. \quad (3.6.1)$$

$$F(x) = k^2\vartheta^2b^2(1-\xi^2)^3 \cdot \sum_0^2 M_n\xi^n \quad .. \quad .. \quad .. \quad .. \quad .. \quad .. \quad .. \quad (3.6.2)$$

$$-\frac{v_x}{Uk^2\vartheta^2} = \ln\frac{2(1-\xi^2)^{1/2}}{\rho}(1-\xi^2)\cdot\sum_0^4 P_n''\xi^n - \sum_0^6 K_n''\xi_n \quad .. \quad .. \quad .. \quad .. \quad (3.6.3)$$

$$\frac{v_r^2}{2U^2k^2\vartheta^2} = (1-\xi^2)\cdot\left(\sum_0^3 S_n'''\xi^n\right)^2 : 8\sum_0^2 M_n\xi^n \quad .. \quad .. \quad .. \quad .. \quad .. \quad (3.6.4)$$

n	K_n''	P_n''	S_n'''
0	$\frac{21}{4}M_0 \quad -\frac{29}{12}M_2$	$3M_0 \quad -M_2$	M_1
1	$\frac{75}{4}M_1$	$9M_1$	$-6M_0 \quad +2M_2$
2	$-\frac{69}{2}M_0 \quad +\frac{85}{2}M_2$	$-15M_0 \quad +17M_2$	$-7M_1$
3	$-\frac{131}{2}M_1$	$-21M_1$	$-8M_2$
4	$\frac{125}{4}M_0 \quad -\frac{431}{4}M_2$	$-28M_2$	—
5	$\frac{959}{20}M_1$	—	—
6	$\frac{343}{5}M_2$	—	—

4. *Examples.*—4.1. *General Remarks.*—The purpose of the twelve examples given below is, first of all, to exhibit the effects of fundamental geometric characteristics on the velocity distribution. It was not intended to produce shapes for immediate practical application, and only four bodies considered (shown in Figs. 7, 8, 12 and 14) may pretend to resemble those used in design. It may be seen, however, that the modest analytical means utilized in this report are amply sufficient for representing any required shape and for determining quickly the corresponding velocity distribution.

The accuracy of the method has been tested on the first example, that of ellipsoids of revolution, for which a simple exact solution exists. It appears (Fig. 16) that the accuracy is very satisfactory for small thickness ratios (up to $\vartheta = 0{\cdot}16$, say) but it deteriorates gradually for further increasing ϑ: *e.g.*, the error for $\vartheta = 0{\cdot}28$ is quite appreciable (*see* Fig. 17). Nevertheless, the diagrams of velocity distribution in all examples have been determined up to $\vartheta = 0{\cdot}28$ (for seven different values of thickness ratio in each case). It is believed that, in spite of poorer accuracy at higher values of ϑ, the diagrams should be at least qualitatively correct, and instructive as to the general trend of changes.

4.2. *Elongated Ellipsoids of Revolution* (*Figs.* 3, 16, 17).—The equation of the meridian line is:

$$\rho = \vartheta(1 - \xi^2)^{1/2}, \quad \ldots \quad (4.2.1)$$

which is a particular case of (3.1.7), with:

$$k = B_0 = 1; \qquad B_1 = B_2 = \ldots = 0. \quad \ldots \quad (4.2.2)$$

The formulae (3.1.10) and (3.1.11) give:

$$-\frac{v_x}{U} = \vartheta^2\left(\ln\frac{2}{\vartheta} - \frac{1}{1-\xi^2}\right); \quad \ldots \quad (4.2.3)$$

$$\frac{v_r^2}{2U^2} = \frac{\vartheta^2}{2}\,\frac{\xi^2}{1-\xi^2}. \quad \ldots \quad (4.2.4)$$

The graphs are given in Figs. 3 and 3a. It is seen that the contribution of radial velocity components is of little importance in this case and, of course, the effect on the maximum supervelocity ratio is nil. The latter occurs at $\xi = 0$ and amounts to:

$$\delta = (\Delta V/U)_{\max} = \vartheta^2\left(\ln\frac{2}{\vartheta} - 1\right). \quad \ldots \quad (4.2.5)$$

The exact formula for δ in this case is derived in the Appendix, and the exact and appropriate numerical results compared in Figs. 16 and 17.

4.3. *Simple Symmetrical Bodies with Pointed Nose and Tail End* (*parabolic meridian line*; *Fig.* 4).—The equation of the meridian line is:

$$\rho = \vartheta(1 - \xi^2), \quad \ldots \quad (4.3.1)$$

which is a particular case of (3.3.1), with:

$$k = E_0 = 1; \qquad E_1 = E_2 = \ldots = 0. \quad \ldots \quad (4.3.2)$$

The formulae (3.3.3) and (3.3.4) yield:

$$-\frac{v_x}{U} = \vartheta^2(1 - 3\xi^2)\left(2\ln\frac{2}{\vartheta(1-\xi^2)^{1/2}} - 3\right); \quad \ldots \quad (4.3.3)$$

$$\frac{v_r^2}{2U^2} = 2\vartheta^2\xi^2. \quad \ldots \quad (4.3.4)$$

The graphs (Figs. 4 and 4a) show that the contribution of v_r is more appreciable. The maximum supervelocities still occur at $\xi = 0$ for small and moderate thickness ratios but, at $\vartheta = 0{\cdot}28$, a small concavity makes appearance on the curve of Fig. 4a. If ϑ is not large, the maximum supervelocity ratio is given by:

$$\delta = \vartheta^2 \left(2 \ln \frac{2}{\vartheta} - 3\right). \quad .. \quad .. \quad .. \quad .. \quad .. \quad .. \quad .. \quad .. \quad (4.3.5)$$

This is appreciably more than (4.2.5), especially for very small values of ϑ, but not for $\vartheta = 0{\cdot}28$.

4.4. *Simple Symmetrical Bodies with Cusped Nose and Tail End* (*Fig.* 5).—The ordinary (semi-cubic) cusps are obtained by putting:

$$\rho = \vartheta(1 - \xi^2)^{3/2}, \quad .. \quad .. \quad .. \quad .. \quad .. \quad .. \quad .. \quad .. \quad (4.4.1)$$

which is a particular case of (3.6.1), with:

$$k = M_0 = 1; \qquad M_1 = M_2 = 0. \quad .. \quad .. \quad .. \quad .. \quad .. \quad (4.4.2)$$

The formulae (3.6.3) and (3.6.4) yield:

$$-\frac{v_x}{U} = \vartheta^2 \left[3(1 - \xi^2)(1 - 5\xi^2) \ln \frac{2}{\vartheta(1 - \xi^2)} - \tfrac{1}{4}(21 - 138\xi^2 + 125\xi^4)\right]; \quad .. \quad (4.4.3)$$

$$\frac{v_r^2}{2U^2} = \frac{9}{2}\vartheta^2\xi^2(1 - \xi^2). \quad .. \quad .. \quad .. \quad .. \quad .. \quad .. \quad .. \quad .. \quad (4.4.4)$$

The graphs are given in Figs. 5 and 5a. It is seen that the contribution of v_r is important, especially for larger values of ϑ. If this contribution were neglected, we should obtain the paradoxical result represented by the curves of $(-v_x/U)$ in Fig. 5, where the maximum supervelocity seems to increase with ϑ only up to about $\vartheta = 0{\cdot}21$, and to decrease later with further increasing thickness ratio. The Fig. 5a shows that, for large values of ϑ, the maximum supervelocities occur in front of and behind the position of maximum thickness, while there is a considerable slowing down of the flow at the thickest central part of the body. Such a behaviour should be expected in this case. The true maximum supervelocity always increases with ϑ. It is clear that the shape of Fig. 5b is disadvantageous at high ϑ.

If ϑ is not large (up to about $0{\cdot}20$), the maximum supervelocity ratio is obtained by putting $\xi = 0$ in (4.4.3), and we have:

$$\delta = \vartheta^2 \left(3 \ln \frac{2}{\vartheta} - \frac{21}{4}\right); \quad .. \quad .. \quad .. \quad .. \quad .. \quad .. \quad .. \quad .. \quad (4.4.5)$$

for higher values of ϑ, no simple expression for δ can be found.

It may be noticed that, contrary to the two previous examples, the supervelocity does not become $(-\infty)$ at $\xi = \pm 1$, but remains finite negative:

$$\left(\frac{\Delta V}{U}\right)_{\xi = \pm 1} = -2\vartheta^2. \quad .. \quad .. \quad .. \quad .. \quad .. \quad .. \quad .. \quad .. \quad (4.4.6)$$

This was to be expected, as a cusp is not a stagnation point. The approximate method applies at the cusp, while it fails at a rounded or pointed nose.

4.5. *Simple Symmetrical Bodies with Strongly Cusped Nose and Tail End* (*Fig.* 6).—We obtain stronger cusps by raising the power of $(1 - \xi^2)$ in the equation of meridian line once more, *i.e.*, by putting:

$$\rho = \vartheta(1 - \xi^2)^2. \quad .. \quad .. \quad .. \quad .. \quad .. \quad .. \quad .. \quad .. \quad (4.5.1)$$

This is again a particular case of (3.6.1), with:

$$k = M_0 = 1; \qquad M_1 = 0; \qquad M_2 = -1. \quad .. \quad .. \quad .. \quad .. \quad .. \quad (4.5.2)$$

We get from (3.6.3) and (3.6.4):

$$-\frac{v_x}{U} = \vartheta^2\left[4(1-\xi^2)^2(1-7\xi^2)\ln\frac{2}{\vartheta(1-\xi^2)^{3/2}} - \left(\frac{23}{3} - 77\xi^2 + 139\xi^4 - \frac{343}{5}\xi^6\right)\right]; \quad (4.5.3)$$

$$\frac{v_r^2}{2U^2} = 8\vartheta^2\xi^2(1-\xi)^2. \quad .. \quad .. \quad .. \quad .. \quad .. \quad .. \quad .. \quad .. \quad (4.5.4)$$

The graphs will be found in Figs. 6 and 6a. They are similar to the previous ones, with even more exaggerated features. The maximum supervelocity occurs at $\xi = 0$ only when ϑ does not exceed about 0·16, and only then δ is represented by the simple formula:

$$\delta = \vartheta^2\left(4\ln\frac{2}{\vartheta} - \frac{23}{3}\right). \quad .. \quad .. \quad .. \quad .. \quad .. \quad .. \quad .. \quad .. \quad (4.5.5)$$

The negative supervelocity ratio at both cusps is now:

$$\left(\frac{\Delta V}{U}\right)_{\xi=\pm 1} = -\frac{16}{15}\vartheta^2. \quad .. \quad .. \quad .. \quad .. \quad .. \quad .. \quad .. \quad .. \quad (4.5.6)$$

4.6. *Simple Bodies with Rounded Nose and Pointed Tail End* (*Figs.* 7, 8).—A family of such bodies may be defined, *e.g.*, by the following equation of the meridian line:

$$\rho = k\vartheta(1+\xi)(1+\lambda\xi)(1-\xi)^{1/2}, \quad .. \quad .. \quad .. \quad .. \quad .. \quad .. \quad (4.6.1)$$

λ being an arbitrary parameter which permits to vary the position of maximum thickness. Denoting by m the value of ξ at which ρ becomes maximum, we find easily:

$$\lambda = \frac{3m-1}{2+m-5m^2} \quad .. \quad .. \quad .. \quad .. \quad .. \quad .. \quad .. \quad .. \quad (4.6.2)$$

and the distance of the thickest cross-section from the nose, expressed as percentage of the length, will be:

$$p = 50(1-m) \quad .. \quad .. \quad .. \quad .. \quad .. \quad .. \quad .. \quad .. \quad .. \quad (4.6.3)$$

The coefficient k will be found from the formula:

$$1/k^2 = (1+m)^2(1+\lambda m)^2(1-m). \quad .. \quad .. \quad .. \quad .. \quad .. \quad .. \quad (4.6.4)$$

A few numerical values are given in the following table:

p (per cent)	m	λ	k^2	k
20	0·6	1	0·38147	0·61763
25	0·5	0·4	0·61728	0·78567
30	0·4	0·125	0·77128	0·87823
$33\frac{1}{3}$	$\frac{1}{3}$	0	0·84375	0·91856
35	0·3	−0·05405	0·87341	0·93456
40	0·2	−0·2	0·94190	0·97052
45	0·1	−0·34146	0·98435	0·99214
50	0	−0·5	1	1

The formula (4.6.1) is a particular case of (3.2.1), with:

$$D_0 = 1; \qquad D_1 = 2\lambda; \qquad D_2 = \lambda^2; \qquad D_3 = D_4 = \ldots = 0; \quad .. \quad .. \quad (4.6.5)$$

hence we get from (3.2.3) and (3.2.4):

$$-\frac{v_x}{Uk^2\vartheta^2}=\left[(1-2\lambda-\lambda^2)+3(1+2\lambda-\lambda^2)\xi+6(2\lambda+\lambda^2)\xi^2+10\lambda^2\xi^3\right].\ln\frac{2}{k\vartheta(1+\lambda\xi)(1+\xi)^{1/2}}$$
$$-\frac{1}{1-\xi}\cdot\left[(1-4\lambda-2\lambda^2)+(3+12\lambda-5\lambda^2)\xi-(3-12\lambda-17\lambda^2)\xi^2\right.$$
$$\left.-\left(18\lambda-\frac{28}{3}\right)\xi^3-\frac{55}{3}\lambda^2\xi^4\right]. \quad .. \quad .. \quad .. \quad .. \quad .. \quad .. \quad (4.6.6)$$

$$\frac{v_r^2}{2U^2k^2\vartheta^2}=\frac{[(1+2\lambda)-(3-\lambda)\xi-5\lambda\xi^2]^2}{8(1-\xi)}. \quad .. \quad .. \quad .. \quad .. \quad .. \quad .. \quad (4.6.7)$$

Two examples of this family have been considered:—

(a) $\lambda=0, p=33\frac{1}{3}$ *per cent.*—In this case the formulae become particularly simple:

$$-\frac{v_x}{U}=0\cdot84375\vartheta^2\left[(1+3\xi)\ln\frac{2}{\vartheta(0\cdot84375(1+\xi))^{1/2}}-\frac{1+3\xi-3\xi^2}{1-\xi}\right]; \quad .. \quad (4.6.8)$$

$$\frac{v_r^2}{2U^2}=0\cdot10547\,\vartheta^2\frac{(1-3\xi)^2}{1-\xi}. \quad .. \quad .. \quad .. \quad .. \quad .. \quad .. \quad .. \quad (4.6.9)$$

The graphs are given in Figs. 7 and 7a. The most interesting feature is the location of maximum supervelocity. It is seen that it varies considerably with thickness ratio. When the latter is quite small, the maximum supervelocity occurs far in front of the thickest section (at about 15 per cent of the length), but it moves backwards, up to nearly 40 per cent, when ϑ increases to 0·28.

(b) $\lambda=-0\cdot2$; $p=40$ *per cent.*—Here we have:

$$-\frac{v_x}{U}=0\cdot9419\vartheta^2\left[(1\cdot36+1\cdot68\xi-2\cdot16\xi^2+0\cdot4\xi^3).\ln\frac{2}{0\cdot97052\vartheta(1-0\cdot2\xi)(1+\xi)^{1/2}}\right.$$
$$\left.-\frac{1\cdot72+0\cdot4\xi-4\cdot72\xi^2+3\cdot9733\xi^3-0\cdot7333\xi^4}{1-\xi}\right]; \quad .. \quad .. \quad .. \quad (4.6.10)$$

$$\frac{v_r^2}{2U^2}=\frac{0\cdot1177\vartheta^2(0\cdot6-3\cdot2\xi+\xi^2)^2}{1-\xi}. \quad .. \quad .. \quad .. \quad .. \quad .. \quad .. \quad (4.6.11)$$

The graphs (Figs. 8 and 8a) are similar to the previous ones, but the maximum supervelocities are somewhat smaller (not appreciably exceeding those for ellipsoids, Fig. 3a), and their location varies only very little with thickness ratio.

4.7. *Simple Bodies with Rounded Nose and Cusped Tail End* (*Fig.* 9).—Let us consider the simplest meridian line of the type required, *i.e.*, put in (3.4.1):

$$H_0=1; \quad H_1=H_2=\ldots=0; \quad k=1. \quad .. \quad .. \quad .. \quad .. \quad (4.7.1)$$

The equation of the meridian line is then:

$$\rho=k\vartheta(1+\xi)(1-\xi^2)^{1/2}, \quad .. \quad .. \quad .. \quad .. \quad .. \quad .. \quad .. \quad (4.7.2)$$

and the abscissa corresponding to the maximum ordinate is easily found:

$$m=0\cdot5, \text{ whence } p=25 \text{ per cent.} \quad .. \quad .. \quad .. \quad .. \quad .. \quad .. \quad (4.7.3)$$

The coefficient k is:

$$k=\frac{1}{(1+m)(1-m^2)^{1/2}}=0\cdot76980, \text{ and } k^2=0\cdot59259. \quad .. \quad .. \quad (4.7.4)$$

The formulae for two supervelocity components are obtained from (3.4.3) and (3.4.4):

$$-\frac{v_x}{U} = 0{\cdot}59259\vartheta^2\left[6\xi(1+\xi)\ln\frac{2}{0{\cdot}7698\vartheta(1+\xi)} + \frac{1-9\xi-3\xi^2+9\xi^3}{1-\xi}\right]; \quad .. \quad (4.7.5)$$

$$\frac{v_r^2}{2U^2} = \frac{0{\cdot}2963\vartheta^2(1+\xi)(1-2\xi)^2}{1-\xi}. \quad .. \quad .. \quad .. \quad .. \quad .. \quad .. \quad (4.7.6)$$

The graphs are given in Figs. 9 and 9a. The contribution of v_r is rather significant in this case. The effect of the cusp, as compared with the pointed tail end (Figs. 7a and 8a), is to produce a wide region of considerable negative supervelocities in the rear of the body, and to increase the peak supervelocity appreciably.

4.8. *Nearly Cylindrical Symmetrical Bodies with Rounded Nose and Tail End.*—A simple example of such bodies (Fig. 10b) is obtained by putting:

$$\rho = \vartheta(1-\xi^4)^{1/2} = \vartheta\{(1-\xi^2)(1+\xi^2)\}^{1/2}. \quad .. \quad .. \quad .. \quad .. \quad .. \quad (4.8.1)$$

This is a particular case of (3.1.7), with:

$$k = 1; \qquad B_0 = B_2 = 1; \qquad B_1 = B_3 = B_4 = \ldots = 0. \quad .. \quad .. \quad (4.8.2)$$

The formulae (3.1.10) and (3.1.11) give:

$$-\frac{v_x}{U} = \vartheta^2\left[6\xi^2\ln\frac{2}{\vartheta(1-\xi^2)^{1/2}} + \frac{1-12\xi^2+9\xi^4}{1-\xi^2}\right]; \quad .. \quad .. \quad .. \quad .. \quad (4.8.3)$$

$$\frac{v_r^2}{2U^2} = \frac{2\vartheta^2\xi^6}{1-\xi^4}. \quad .. \quad .. \quad .. \quad .. \quad .. \quad .. \quad .. \quad .. \quad .. \quad (4.8.4)$$

The Figs. 10 and 10a show the supervelocity distribution. The curves are very different from all the previous ones. The maxima occur near the nose and tail end, and there is a considerable slowing down of the flow near the centre, especially for small thickness ratios. For larger ϑ, the concavity becomes less conspicuous and finally disappears so that, for instance, at $\vartheta = 0{\cdot}32$, the maximum occurs at $\xi + 0$.

There is a strikingly simple formula for the supervelocity at $\xi = 0$:

$$(\Delta V/U)_{\xi=0} = \vartheta^2, \quad .. \quad .. \quad .. \quad .. \quad .. \quad .. \quad .. \quad .. \quad .. \quad (4.8.5)$$

but the practical meaning of this formula is small. The true maximum may be several times greater than this. Only for large ϑ (from $\vartheta = 0{\cdot}28$ upwards, say) may (4.8.5) be considered as an approximate maximum, but we cannot expect a good accuracy for such high thickness ratios.

4.9. *Nearly Cylindrical Symmetrical Bodies with Pointed Nose and Tail End* (*Fig.* 11).—The equations of meridian lines for such bodies may be obtained from (3.3.1) by choosing the coefficients E_n in such a way that as many derivatives of (3.3.1) as possible become $= 0$ at $\xi = 0$. This means that a certain (odd) number of coefficients S_n' (in sub-section 3.3) must be $= 0$. The simplest case is obtained by putting:

$$k = 1; \qquad E_0 = 1; \qquad E_2 = 2; \qquad E_1 = E_3 = 0. \quad .. \quad .. \quad .. \quad (4.9.1)$$

The equation of the meridian line then becomes:

$$\rho = \vartheta(1-\xi^2)(1+2\xi)^{21/2} \quad .. \quad .. \quad .. \quad .. \quad .. \quad .. \quad .. \quad (4.9.2)$$

(*see* Fig. 11b), and the formulae (3.3.3) and (3.3.4) yield:

$$-\frac{v_x}{U} = \vartheta^2\left[(18\xi^2-30\xi^4)\ln\frac{2}{\vartheta(1+\xi^2-2\xi^4)^{1/2}} + \left(\frac{3}{2}-42\xi^2+\frac{125}{2}\xi^4\right)\right]; \quad .. \quad (4.9.3)$$

$$\frac{v_r^2}{2U^2} = \frac{18\vartheta^2\xi^6}{1+2\xi^2} \quad .. \quad .. \quad .. \quad .. \quad .. \quad .. \quad .. \quad .. \quad .. \quad (4.9.4)$$

The graphs are given in Figs. 11 and 11a, and are instructive. For small ϑ's, the velocity distribution does not differ much from that in the previous examples, there being again concavities in the curves, due to the quasi-cylindrical part. For medium values of ϑ the concavity disappears, and the maximum ΔV occurs at $\xi = 0$. For still higher values of thickness ratio, the curves become very irregular, with additional sharp maxima and deep narrow concavities in the front and in the rear (due to the blunt pointed tips).

At $\xi = 0$, we have again an extremely simple formula for the supervelocity:

$$(\Delta V/U)_{\xi=0} = \tfrac{3}{2}\vartheta^2 , \quad .. \quad .. \quad .. \quad .. \quad .. \quad .. \quad .. \quad .. \quad .. \quad (4.9.5)$$

and this is, approximately, the maximum supervelocity ratio for large ϑ's (upwards of 0·16, say), but not for small ϑ's.

4.10. *Nearly Cylindrical Bodies with Rounded Nose and Pointed Tail End* (*Fig.* 12).—This is an important case, because shapes of this kind are often used in design. The equation of the meridian line must be a special case of (3.2.1). Suppose that the maximum ordinate corresponds to $\xi = m$. We have to fulfil the requirement that, at $\xi = m$, at least three (or possibly 5, 7, etc.) derivatives of (3.2.2) become equal to 0. The simplest solution of this kind can be obtained by keeping only four coefficients D_0, D_1, D_2, D_3 different from zero, thus:

$$\rho = k\vartheta(1+\xi)\{(1-\xi)(D_0 + D_1\xi + D_2\xi^2 + D_3\xi^3)\}^{1/2} , \quad .. \quad .. \quad .. \quad (4.10.1)$$

whence:

$$\frac{F(x)}{k^2\vartheta^2b^2} = (1+\xi-\xi^2-\xi^3)(D_0 + D_1\xi + D_2\xi^2 + D_3\xi^3) . \quad .. \quad .. \quad .. \quad (4.10.2)$$

It may be proved* that, if the coefficients D_0, D_1, D_2, D_3 are:

$$\left.\begin{aligned} D_0 &= 1 + m - 4m^2 - 4m^3 + 3m^4 + 15m^5 - 20m^6 , \\ D_1 &= -1 - m + 4m^2 + 16m^3 - 39m^4 + 45m^5 , \\ D_2 &= 2 + 2m - 26m^2 + 34m^3 - 36m^4 , \\ D_3 &= -2 + 10m - 10m^2 + 10m^3 , \end{aligned}\right\} \quad .. \quad .. \quad .. \quad (4.10.3)$$

then the first derivative of (4.10.2) becomes:

$$\frac{F'(x)}{k^2\vartheta^2b} = 4(1+\xi)(m-\xi)^3(J_0 - J_1\xi) , \quad .. \quad .. \quad .. \quad .. \quad .. \quad .. \quad (4.10.4)$$

where:

$$J_0 = 3 - 9m + 15m^2 - 5m^3 ; \qquad J_1 = 3(1 - 5m + 5m^2 - 5m^3) , \quad .. \quad (4.10.5)$$

so that $F'(mb) = 0$, and also $F''(mb) = 0$ and $F'''(mb) = 0$. The geometrical conditions are thus satisfied. The coefficient k is found easily:

$$1/k^2 = (1+m)^2(1-m)(D_0 + D_1m + D_2m^2 + D_3m^3) , \quad .. \quad .. \quad .. \quad (4.10.6)$$

or better:

$$1/k = (1-m^2)^2\{1+m\}^{1/2} \quad .. \quad .. \quad .. \quad .. \quad .. \quad .. \quad .. \quad (4.10.7)$$

The formula (3.2.3) becomes:

$$-\frac{v_x}{Uk^2\vartheta^2} = 2(m-\xi)^2(Q_0 + Q_1\xi + Q_2\xi^2) \cdot \ln\frac{2(1-\xi^2)^{1/2}}{\rho} - \frac{1}{1-\xi}\sum_0^5 K_n'\xi^n , \quad .. \quad (4.10.8)$$

* The algebraical work required is rather long but does not present any fundamental difficulties.

where:

$$\left.\begin{aligned} Q_0 &= 9 - 27m + 39m^2 - 15m^3 - 10m^4 , \\ Q_1 &= -10(3m - 3m^2 + 7m^3 - 3m^4) , \\ Q_2 &= -15(1 - 5m + 5m^2 - 5m^3) , \end{aligned}\right\} \quad .. \quad .. \quad .. \quad .. \quad .. \quad (4.10.9)$$

and

$$\left.\begin{aligned} K_0' &= -1{\cdot}5 + 1{\cdot}5m + 37{\cdot}5m^2 - 101{\cdot}5m^3 + 153m^4 - 75m^5 - 20m^6 , \\ K_1' &= 1{\cdot}5 - 85{\cdot}5m + 214{\cdot}5m^2 - 158{\cdot}5m^3 - 45m^4 + 315m^5 - 60m^6 , \\ K_2' &= 42 - 60m - 321m^2 + 601m^3 - 855m^4 + 225m^5 + 60m^6 , \\ K_3' &= -42 + 376m - 627m^2 + 521{\cdot}66\,..\,m^3 + 15m^4 - 405m^5 , \\ K_4' &= -62{\cdot}5 + 92{\cdot}5m + 347{\cdot}5m^2 - 494{\cdot}166\,..\,m^3 + 660m^4 , \\ K_5' &= 62{\cdot}5(1 - 5m + 5m^2 - 5m^3) . \end{aligned}\right\} \quad .. \quad (4.10.10)$$

The formula (3.2.1) yields:

$$\frac{v_r^2}{2U^2k^2\vartheta^2} = \frac{2(m - \xi)^6 (J_0 - J_1\xi)^2}{(1 - \xi)(D_0 + D_1\xi + D_2\xi + D_3\xi^3)} . \quad .. \quad .. \quad .. \quad .. \quad .. \quad (4.10.11)$$

One particular case has been studied in detail, corresponding to the value:

$$m = 0{\cdot}2 \quad (i.e., \; p = 40 \text{ per cent}). \quad .. \quad .. \quad .. \quad .. \quad .. \quad (4.10.12)$$

In this case we have:

$$\left.\begin{aligned} k &= 0{\cdot}990528; \quad k^2 = 0{\cdot}981146; \\ D_0 &= 1{\cdot}01632; \quad D_1 = -0{\cdot}96; \quad D_2 = 1{\cdot}5744; \quad D_3 = -0{\cdot}32; \\ Q_0 &= 5{\cdot}024; \quad Q_1 = 5{\cdot}312; \quad Q_2 = -2{\cdot}4; \\ K_0' &= -0{\cdot}29248; \quad K_1' = -8{\cdot}26304; \quad K_2' = 20{\cdot}67584; \quad K_3' = 12{\cdot}1873; \\ K_4' &= -32{\cdot}9973; \quad K_5' = 10; \quad J_0 = 1{\cdot}76; \quad J_1 = 0{\cdot}48 . \end{aligned}\right\} \quad (4.10.13)$$

The meridian line is traced in Fig. 12b, and the velocity distribution curves in Figs. 12 and 12a. It is seen that the quasi-cylindrical part again produces concavities in the curves when ϑ is small. For larger ϑ, these concavities disappear. Another concavity appears then in the rear, but it is much milder than in Fig. 11a, the pointed tip being less blunt in this case.

4.11. *Symmetrical Bodies with Central Waist, Rounded Nose and Tail End* (*Fig.* 13).—It has been suggested[13] that a wing-fuselage junction could be designed to advantage by shaping the fuselage as a body with a waist located so as to coincide with the region of greatest supervelocities of the root region of a swept-back wing, so that they would be compensated by the reduced (or even negative) supervelocities caused by the waist. The problem is complicated by the mutual interference of the wing and body. The first step for a solution is obviously to examine the velocity distribution over ' waisted ' bodies taken alone, and one of the simplest examples is the symmetrical body of Fig. 13b which may be represented by the equation of the meridian line:

$$\rho = k\vartheta(1 - \xi^2)^{1/2} (1 + \nu\xi^2) , \quad .. \quad .. \quad .. \quad .. \quad .. \quad .. \quad .. \quad (4.11.1)$$

this being a particular case of (3.1.7). We have then:

$$B_0 = 1; \quad B_2 = 2\nu; \quad B_4 = \nu^2; \quad B_1 = B_3 = B_5 = B_6 = 0 . \quad .. \quad .. \quad .. \quad (4.11.2)$$

The maximum ρ will occur at $\xi = \pm m$, and it is easily found that:

$$m = \{(2\nu - 1)/3\nu\}^{1/2} , \text{ or } \nu = 1/(2 - 3m^2) . \quad .. \quad .. \quad .. \quad .. \quad .. \quad (4.11.3)$$

The value ρ_{max} must be equal to ϑ, whence:

$$1/k = (1 - m^2)^{1/2}(1 + \nu m^2) = \tfrac{2}{3}(1 + \nu)\{(1 + \nu)/3\nu\}^{1/2} = 2(1 - m^2)^{3/2}/(2 - 3m^2) , \quad (4.11.4)$$

and, the value ρ_w at the waist (for $\xi = 0$) being equal to $k\vartheta$, the coefficient k is simply the 'constriction ratio' $\rho_w/\rho_{\max}$.

The two contributions to the supervelocity are obtained from the formulae (3.1.10) and (3.1.11), by using the table following them and the expressions (4.11.2). We get:

$$-\frac{v_x}{U k^2\vartheta^2} = \left\{(1-2\nu) + (12\nu - 6\nu^2)\xi^2 + 15\nu^2\xi^4\right\} \cdot \ln\frac{2}{k\vartheta(1+\nu\xi^2)}$$
$$-\frac{1}{1-\xi^2}\cdot\left\{\left(1 - 4\nu + \frac{1}{4}\nu^2\right) + \left(24\nu - \frac{64}{3}\nu^2\right)\xi^2\right.$$
$$\left. + \left(\frac{191}{4}\nu^2 - 18\nu\right)\xi^4 - \frac{125}{4}\nu^2\xi^6\right\}; \quad \ldots\ldots\ldots\ldots\ldots\ldots\ldots\ldots \quad (4.11.5)$$

$$\frac{v_r^2}{2U^2k^2\vartheta^2} = \frac{\xi^2(2\nu - 1 - 3\nu\xi^2)^2}{2(1-\xi^2)} \cdot \quad \ldots\ldots\ldots\ldots\ldots\ldots\ldots\ldots \quad (4.11.6)$$

The numerical computation has been done for one particular case only, *i.e.*, $\nu = 1{\cdot}4$, so that:

$$\left.\begin{aligned} m = (3/7)^{1/2} = 0{\cdot}65465; \qquad 1/k = 16/\sqrt{175} = 1{\cdot}20949, \\ \text{constriction ratio} \\ k = 0{\cdot}82680; \qquad k^2 = 175/256 = 0{\cdot}68359, \end{aligned}\right\} \quad \ldots\ldots\ldots \quad (4.11.7)$$

and we have:

$$-\frac{v_x}{U} = k^2\vartheta^2\left[(1{\cdot}8 - 5{\cdot}04\xi^2 - 29{\cdot}4\xi^4)\cdot\ln\frac{k\vartheta(1+1{\cdot}4\xi^2)}{2}\right.$$
$$\left. + \frac{4{\cdot}11 - 2{\cdot}73\xi^2 - 68{\cdot}39\xi^4 + 61{\cdot}25\xi^6}{1-\xi^2}\right]; \quad \ldots\ldots\ldots\ldots\ldots \quad (4.11.8)$$

$$\frac{v_r^2}{2U^2} = 2k^2\vartheta^2\xi^2(0{\cdot}9 - 2{\cdot}1\xi^2)^2/(1-\xi^2). \quad \ldots\ldots\ldots\ldots\ldots \quad (4.11.9)$$

The graphs are given in Figs. 13 and 13a, and they exhibit some interesting features. When the thickness ratio is small, then the maximum supervelocities are located very near to the nose and tail end, well outboard of the positions of maximum thickness, but they move considerably inboard (and beyond maximum thickness) with increasing ϑ. Owing to the strong constriction in the waist, the supervelocities fall deeply towards the centre section where they become approximately nil, or even slightly negative at medium thickness ratios. This is paid for, however, by the serious penalty of, comparatively, very high maximum supervelocities, much higher than in Fig. 3 or Fig. 10. This unpleasant fact is due to the fully rounded end parts of the body which resemble halves of a much thicker body. The feature could be avoided by extending the end parts much further outboard, but this would mean a considerable reduction of thickness ratio in any given case, *i.e.*, an excessive length for a given maximum diameter. If considerable negative supervelocities at the waist centre were aimed at, an even stronger constriction would be needed, but then the maximum supervelocities would become even higher, unless a further extension of the end parts were applied. It is also doubtful whether a deep constriction would be acceptable for constructional reasons, so it is seen that there are serious difficulties to overcome in this sort of design. The problem may be further studied by adding more terms in (4.11.1).

4.12. *Bodies with Rounded Nose, Pointed Tail End, and a Shallow Waist* (*Fig.* 14).—The previous example was chosen in order to exhibit the aerodynamic properties of a deep waist in a simple and characteristic case. The shape of Fig. 13b, however, is far from suitable for a fuselage. In a real design, there will never be a fore-and-aft symmetry, and the tail end will be pointed. Such shapes may, of course, also be represented by suitable algebraic equations, but

the calculations become more complicated. Only one, comparatively simple, case will be analysed here, as illustrated by Fig. 14b. The two maximum diameters of the body are assumed equal, one of them located at mid-axis, and the other one in the front, at $\xi = m$. Only a shallow waist can then be obtained in between, if a simple function is to be used, and excessive local curvature avoided. A suitable equation of the meridian line will be a particular case of (3.2.1), and may be written thus:

$$\rho = \vartheta(1 + \xi)\{(1 - \xi)(1 - \xi + D_2\xi^2 + D_3\xi^3)\}^{1/2}, \quad .. \quad .. \quad .. \quad .. \quad (4.12.1)$$

which corresponds to the assumption:

$$k = 1, \quad D_0 = 1, \quad D_1 = -1, \quad D_4 = D_5 = 0, \quad .. \quad .. \quad .. \quad .. \quad (4.12.2)$$

while two parameters D_2 and D_3 can still be chosen freely. The form of (4.12.1) ensures that ρ becomes maximum at $\xi = 0$ (provided $D_2 < 2$). Assuming now that the second maximum is at $\xi = m$, and is equal to the first one, we obtain, after some calculation:

$$D_2 = \frac{2 + 2m - 7m^2 - m^3 + 2m^4}{(1 + m)(1 - m^2)^2}; \qquad D_3 = \frac{-2 + 4m + m^2 - m^3}{(1 + m)(1 - m^2)^2}. \quad .. \quad (4.12.3)$$

The abscissa ξ_w corresponding to ρ_w (minimum at the waist) will then be the smaller root of the equation:

$$3(2 - 4m - m^2 + m^3)\xi_w^2 - (6 - 3m - 6m^2 + m^3 + 2m^4)\xi_w + (3m - 3m^2 + 2m^4) = 0, \quad (4.12.4)$$

and will be found to be only slightly greater than $\frac{1}{2}m$; the minimum radius ρ_w will be determined by substituting ξ_w into (4.12.1).

The two contributions to the velocity will be found from (3.2.3) and (3.2.4), where the coefficients should be calculated from the table following those formula, under assumptions (4.12.2) and (4.12.3).

The numerical computation has been performed for one case $m = 0{\cdot}6$, so that:

$$D_2 = \frac{565}{512}, \qquad D_3 = \frac{425}{512}, \qquad \xi_w \simeq 0{\cdot}322, \quad .. \quad .. \quad .. \quad .. \quad .. \quad (4.12.5)$$

and we obtain a very weak constriction ratio:

$$\rho_w/\vartheta \simeq 0{\cdot}986.$$

The final formulae for the supervelocity contributions become:

$$-\frac{v_x}{U\vartheta^2} = \frac{4{\cdot}59 - 29{\cdot}7\xi - 22{\cdot}32\xi^2 + 99\xi^3 + 63{\cdot}75\xi^4}{5{\cdot}12} \cdot \ln\frac{2(1 - \xi^2)^{1/2}}{\rho}$$
$$- \frac{2{\cdot}049 - 29{\cdot}769\xi + 5{\cdot}538\xi^2 + 98{\cdot}742\xi^3 - 19{\cdot}475\xi^4 - 53{\cdot}125\xi^5}{2{\cdot}048\,(1 - \xi)}; \quad .. \quad (4.12.7)$$

$$\frac{v_r^2}{2U^2\vartheta^2} = \frac{225\xi^2\,(0{\cdot}6 - \xi)^2\,(0{\cdot}53 - 1{\cdot}31\xi - 0{\cdot}85\xi^2)^2}{102{\cdot}4\,(1 - \xi)(0{\cdot}512 - 0{\cdot}512\xi + 0{\cdot}565\xi^2 + 0{\cdot}425\xi^3)}. \quad .. \quad .. \quad (4.12.8)$$

The graphs are given in Figs. 14 and 14a. It is seen that the maximum supervelocities are generally even greater than in the previous case (Fig. 13a), not to mention the comparable cases shown in Figs. 7a and 12a. At the same time, the effect of the shallow waist is much smaller than in the previous case, the reduced supervelocities in the waist region being always positive and not inconsiderable. A striking feature is that the region of smallest supervelocities travels fast backwards with increasing thickness ratio, up to far behind the waist. The problem merits further examination, and may be studied by varying the numerical values of coefficients in (4.12.1), or possibly adding more terms.

5. *Practical Conclusions.*--Although the material assembled in the previous section and illustrated by Figs. 3 to 14 does not pretend to exhaust all geometric and aerodynamic possibilities, several general conclusions may be drawn from the examination and comparison of the results so far obtained:—

(a) The most striking feature of the diagrams is the wide *diversity* of the supervelocity diagrams. All bodies considered are more or less ' streamlined ', and yet the diagrams differ considerably from each other. In many cases, an apparently smooth meridian curve leads to a definitely disadvantageous velocity distribution. This shows that the ' designer's eye ' may not suffice for avoiding aerodynamically faulty design, and that a preliminary investigation of each projected body by means of the method suggested may prevent faults and help to obtain better results. The application of the method requires a representation of the meridian line by an algebraic equation, but this is always to be recommended and, apart from a little elementary algebraic work, does not mean any limitation in practice.

(b) The above conclusion is reinforced when we consider the *effect of thickness*. It has been mentioned already in the Introduction and section 2 that the velocity curves for different values of ϑ are generally not similar. Now, the examples show that they may change with ϑ in quite an unexpected way (Figs. 4, 5, 6, 10, 11, 13). The number of maxima and their location may be altered, and a profile, excellent at small ϑ, may become bad at large ϑ (Fig. 5); or *vice versa* (Fig. 12). It is no longer possible, as in wing theory, to scale up the velocity distribution in any simple manner with thickness ratio.

(c) The *contribution of* v_r, neglected heretofore by all approximate methods, is seen to be quite important not only theoretically but, in many cases, in a very tangible way. In some examples (Figs. 4, 7 to 9, 10, 12, 13) the effect is only quantitative, *e.g.*, widening the region of positive supervelocities without affecting the general course of curves or changing their maxima appreciably; but, in some other cases, the contribution of v_r alters the picture beyond recognition, *e.g.*, moving the position of maximum supervelocity or even revealing new and higher maxima (Figs. 5 and 5a, 6 and 6a, 11 and 11a, 14 and 14a). This contribution should therefore not be neglected.

(d) The number, positions and values of the *supervelocity maxima*, important both from the point of view of critical Mach numbers and of the behaviour of the boundary layer, is affected by both the shape of meridian line and the thickness ratio. The maximum supervelocity ratio δ for a given ϑ varies in a wide range, and this variation is best exhibited in the comparative diagram of Fig. 15, where δ is plotted against ϑ for all twelve shapes examined. The curves often cross each other. The maxima not seldom occur far from the points of maximum thickness, and may be located in front of or behind them, often depending on ϑ. For some cases, as those of Figs. 4, 5, 6, 10, additional broken lines in Fig. 15 show the local *minima* actually occurring at maximum thickness points, as against the maxima which are located elsewhere. It may be mentioned that the ellipsoids of revolution present the lowest maxima at all thickness ratios, and this shape seems to be most advantageous from this point of view (although usually inapplicable because of other considerations), similarly as the ellipse in two dimensions. It is advisable to try to use shapes for which the maxima exceed only slightly those of ellipsoids, especially for high subsonic operation. It is generally required in addition, both for low and high speed, that there should be only a single velocity peak, as far back as possible, followed by low adverse slope.

(e) The effect of *shaping the nose and tail end* is, of course, considerable. This may be studied in all examples, but some of them (Figs. 4 to 6, 9 to 11) have been presented mainly with the purpose of exhibiting these effects. It is seen that *cusps*, in spite of their apparent advantage of being *not stagnation points and* therefore seemingly ' very streamlined ', do not produce any advantage. They do not contribute even to reducing the adverse slope of velocity curves, while causing unwanted reversed peaks at the very ends (Figs. 5, 6, 9) and often, especially at high ϑ, they result in high (sometimes split) maxima (Figs. 5 and 6). This may be explained by the fact that the air, having encountered little impediment initially, must then break through past the rapidly increasing thickness. At high ϑ, the region of maximum thickness is comparatively

sheltered, and thus exhibits the unexpected ' semi-stagnation '. The cusps are, of course, undesirable for constructional reasons, but they may be considered as extreme representatives of regions of strong curvature which, accordingly, should also be avoided. As to the *rounded and pointed extremities*, they do not produce widely different effects for otherwise smooth profiles (Figs. 3, 4, 7, 8), the former being normally recommended for noses, the latter for tail ends. The pointed tail end may, however, cause considerable additional peaks when combined with nearly cylindrical middle-bodies of large thickness ratios (Figs. 10, 11, 12).

(f) A particular interest should be attached to *nearly cylindrical bodies* (Figs. 10, 11, 12). They are often used because of attractive constructional features. Our Figures show, however, that their velocity curves are not quite satisfactory. At small or moderate ϑ, they show definite ' semi-stagnation ' regions in their cylindrical parts, with undulating course; those vanish, curiously, at high ϑ, but reappear more threateningly near the pointed extremities (Figs. 11, 12). A particular *warning* should be given *against strictly cylindrical shape* with affixed rounded or pointed ends, because, as known, the discontinuities of curvature cause particularly bad velocity curves, with vertical inflexion tangents.

(g) As mentioned in connection with examples 4.11 and 4.12 (Figs. 13, 14), the semi-stagnation in middle parts may be sought on purpose, by introducing central or eccentric waists, aiming at an advantageous solution of the *wing junction*. The aim of reducing supervelocities locally may thus be attained, with no theoretical limits, at the cost, however, of considerable rise in maximum supervelocities elsewhere. The problem is complicated and requires a very careful and difficult investigation, if critical Mach numbers are to be appreciably reduced without causing troubles with boundary layer and local burbles.

(h) The new method will find a wide scope when applied to *compressible subsonic flow* past bodies of revolution. This subtle problem has caused a good deal of controversies (R. & M. 1909[7] and 2624[12], and Ref. 14), but at present may be regarded as solved by the *generalized three-dimensional similarity law* in its specific form for axially symmetrical flow. According to this, the compressible flow at Mach number M past a given body (thickness ratio ϑ) may be obtained from the incompressible flow past an ' analogous ' body of a smaller thickness ratio $\vartheta(1 - M^2)^{1/2}$ by increasing the induced axial velocity components (v_x) in the ratio $1/(1 - M^2)$, and the radial ones (v_r) in the ratio $1/(1 - M^2)^{1/2}$. A fortunate coincidence is that the latter's contribution to ΔV is proportional to v_r^2, hence increases in the same proportion as v_x, and therefore the resulting velocity curves all belong to the same families of ' incompressible ' curves as calculated in our examples. The critical Mach numbers may thus be calculated simply on the general lines of Ref. 15, but it is not proposed to enlarge on the subject here.

LIST OF SYMBOLS

A	Area of the cross-section of a body of revolution
$A_0, A_1, A_2, \ldots$	Coefficients, *see* (3.1.2)
$B_0, B_1, B_2, \ldots$	Coefficients, *see* (3.1.7)
b	Half-length of the body of revolution
$D_0, D_1, D_2, \ldots$	Coefficients, *see* (3.2.1)
E	Constant, *see* (A.5)
$E_0, E_1, E_2, \ldots$	Coefficients, *see* (3.3.1)
e	Eccentricity of an ellipsoid of revolution
$F(x)$	Function of x expressing r^2, *see* (2.2)
$H_0, H_1, H_2, \ldots$	Coefficients, *see* (3.4.1)
$I_k, I_0, I_1, I_2, \ldots$	Definite integrals, *see* (2.14)
J_0, J_1	Portmanteau symbols, *see* (4.10.5)
$K_0, K_1, K_2, \ldots$	Coefficients, *see* (3.1.5)
$K_0', K_1', K_2', \ldots$	Coefficients, *see* (3.2.3) and (3.4.3)
$K_0'', K_1'', K_2'', \ldots$	Coefficients, *see* (3.3.3), (3.5.3.) and (3.6.3)
k	Coefficient, *see* (3.1.2)
$L_0, L_1, L_2, \ldots$	Coefficients, *see* (3.5.1)
$M_0, M_1, M_2, \ldots$	Coefficients, *see* (3.6.1)
m	Value of ξ at which r becomes maximum
N	Constant, *see* (A.19)
n	Index, *see* (3.1.4)
$P_0, P_1, P_2, \ldots$	Coefficients, *see* (3.1.10)
P_0', P_1', P_2'	Coefficients, *see* (3.4.3)
P_0'', P_1'', P_2''	Coefficients, *see* (3.6.3)
p	Auxiliary variable, *see* (2.13)
Q_0, Q_1, Q_2	Coefficients, *see* (4.10.9)
q	Local source intensity per unit length
R	Distance, *see* Fig. 1
$R_0, R_1, R_2, \ldots$	Coefficients, *see* (3.1.11)
r	Radial co-ordinate of a point on the body surface
r_{el}	r for an ellipsoid of revolution
S_0, S_1, S_2	Coefficients, *see* (3.2.4)
S_0', S_1', S_2'	Coefficients, *see* (3.3.4)
S_0'', S_1'', S_2''	Coefficients, *see* (3.5.4)
S_0''', S_1''', S_2'''	Coefficients, *see* (3.6.4)

LIST OF SYMBOLS—*continued*

T_0, T_1, T_2	Coefficients, *see* (3.4.4)
U	Undisturbed velocity of the air flow
V	Resultant velocity
v	Induced velocity
v_r	Radial component of v
v_x	Axial component of v
x	Axial co-ordinate of a point on the body surface, positive forwards
$\bar{x}$	Axial co-ordinate of a source element on the axis
α	Angle of slope of a tangent to an ellipsoid
δ	Maximum supervelocity ratio, *see* (4.2.5)
ζ	Curvilinear co-ordinate, *see* (A.2)
ζ_0	Value of ζ on the surface of an ellipsoid
θ	Angle, *see* Fig. 1
$\vartheta = r_{\max}/b$	Thickness ratio
λ	Parameter, *see* (4.6.1)
μ	Curvilinear co-ordinate, *see* (A.2)
ν	Parameter, *see* (4.11.1)
$\xi = x/b$	Non-dimensional axial co-ordinate
$\rho = r/b$	Non-dimensional radial co-ordinate
ρ_w	Minimum value of ρ at the waist
Φ	Velocity potential, *see* (A.4)

REFERENCES

No.	*Author*	*Title, etc.*
1	H. Lamb	*Hydrodynamics*, Fifth Edition. Cambridge University Press. 1924.
2	G. Fuhrmann	Theoretische und experimentelle Untersuchungen an Ballon-Modellen. *Jahrbuch* 1911–12 *der Motorluftschiff-Studiengesellschaft*, p. 65.
3	Th. von Kármán	Berechnung der Druckverteilung an Luftschiffkörpern. Abhandlungen aus dem Aerodynamischen Institut a.d. T. H. Aachen. No. 6. Berlin. 1927.
4	S. Neumark	Sur l'écoulement de fluide parfait contournant les corps de révolution à une pointe effilée. *Proceedings of the 3rd International Congress for Applied Mechanics*. Stockholm. 1930.
5	C. Kaplan	Potential Flow about Elongated Bodies of Revolution. N.A.C.A. Report No. 516. 1935.
6	H. B. Squire	Review of the Calculations of Low Drag Wing Sections. Appendix II, 1. A.R.C. 5865. (Unpublished.)
7	S. Goldstein and A. D. Young ..	The Linear Perturbation Theory of Compressible Flow with Applications to Wind Tunnel Interference. R. & M. 1909. July, 1943.
8	A. D. Young and P. R. Owen ..	A Simplified Theory for Streamline Bodies of Revolution, and its Application to the Development of High Speed Shapes. R. & M. 2071. July, 1943.
9	M. J. Lighthill	Supersonic Flow past Bodies of Revolution. R. & M. 2003. January, 1945.
10	A. D. Young and E. Young ..	A Family of Streamline Shapes Suitable for High Speed or Low Drag Requirements. R. & M. 2204. August, 1945.
11	S. Neumark	Velocity Distribution on Straight and Sweptback Wings of Small Thickness and Infinite Aspect Ratio at Zero Incidence. R. & M. 2713. May, 1947.
12	A. D. Young and S. Kirkby ..	Application of the Linear Perturbation Theory to Compressible Flow about Bodies of Revolution. *Report No. 11, the College of Aeronautics, Cranfield*. R. & M. 2624. September, 1947.
13	D. Küchemann	Design of Wing Junction, Fuselage and Nacelles to Obtain the Full Benefit of Swept-back Wings at High Mach Number. A.R.C. 11,035. August, 1947. (To be published.)
14	R. V. Hess and Clifford S. Gardner	Study by the Prandtl-Glauert Method of Compressibility Effects and Critical Mach Numbers for Ellipsoids of Various Aspect Ratios and Thickness ratios. N.A.C.A. Technical Note No. 1792. January, 1949.
15	S. Neumark	Critical Mach Numbers for Thin Untapered Swept Wings at Zero Incidence. R. & M. 2821. November, 1949.

APPENDIX

Estimate of Accuracy of the Method for Ellipsoids of Revolution

It has been proved in section 2 that, when using our method for thin bodies of revolution, the boundary conditions on the surface are satisfied with only small errors of the order ϑ^3 on the local slope which is itself small of the order ϑ; also, that the velocity v_x, itself small of the order $\vartheta^2 \ln \vartheta$ and ϑ^2, is determined with errors of the order $\vartheta^4 \ln \vartheta$ and ϑ^4. This seems quite satisfactory. It is desirable, however, to compare numerically the approximate solution with an exact one, at least for one particular shape of not very small thickness ratio, to see how far they agree and what numerical differences take place. A specimen body with rounded nose would be particularly suitable, because then $F''(x)$ has no upper bound within the range $(-b \leqslant x \leqslant b)$, and therefore treating its mean value K (in formula 2.15) as small of the order ϑ^2 may seem doubtful.

Only very few exact solutions have been obtained by potential theory for bodies of revolution with meridian lines expressible by simple algebraical functions. A comparatively easy case is that of elongated ellipsoids of revolution, and its exact solution, due to Heine, and considered by H. Lamb[1], is used below to deduce convenient formulae for velocity distribution.

The semi-axes of the ellipsoid being b and ϑb (Fig. 3b), and the distance OF (from the centre to a focus) being denoted by be, where

$$\text{eccentricity} \quad e = (1 - \vartheta^2)^{1/2}, \qquad \text{whence} \quad \vartheta = (1 - e^2)^{1/2}, \quad \ldots \quad \ldots \quad \ldots \quad (A.1)$$

auxiliary curvilinear co-ordinates ζ and μ are introduced, connected with the cylindrical ones x and r by the relationships

$$\left.\begin{aligned} x &= be\zeta\mu\,, \\ r^2 &= b^2e^2(\zeta^2 - 1)(1 - \mu^2) \end{aligned} \qquad (\zeta \geqslant 1,\ 0 \leqslant \mu \leqslant 1) \right\} \ldots \quad \ldots \quad (A.2)$$

The loci $\zeta = \text{const.}$ are elongated ellipsoids, of semi-axes $be\zeta$ and $be(\zeta^2 - 1)^{1/2}$; while those $\mu = \text{const.}$ are hyperboloids of two sheets, of semi-axes $be\mu$ and $be(1 - \mu^2)^{1/2}$. The given ellipsoid corresponds to $\zeta = \zeta_0$, where:

$$\zeta_0 = 1/e\,. \quad \ldots \quad \ldots \quad \ldots \quad \ldots \quad \ldots \quad \ldots \quad \ldots \quad \ldots \quad \ldots \quad (A.3)$$

The velocity field produced by the motion of the ellipsoid with a uniform velocity U in the direction of the positive x axis is then (*see* Ref. 1, page 132, form. 4):

$$\Phi = -\frac{Ube}{E}\mu\left(\zeta \ln\frac{\zeta + 1}{\zeta - 1} - 2\right), \quad \ldots \quad \ldots \quad \ldots \quad \ldots \quad \ldots \quad (A.4)$$

where the constant E is:

$$E = \frac{2\zeta_0}{\zeta_0^2 - 1} - \ln\frac{\zeta_0 + 1}{\zeta_0 - 1} = \frac{2e}{1 - e^2} - \ln\frac{1 + e}{1 - e}. \quad \ldots \quad \ldots \quad \ldots \quad (A.5)$$

The velocity components v_x and v_r *at an arbitrary point in space* are obtained by differentiating (A.4) partially with respect to x and r:

$$\left.\begin{aligned} v_x = \frac{\partial\Phi}{\partial x} &= -\frac{Ube}{E}\left[\mu\left(\ln\frac{\zeta + 1}{\zeta - 1} - \frac{2\zeta}{\zeta^2 - 1}\right)\frac{\partial\zeta}{\partial x} + \left(\zeta \ln\frac{\zeta + 1}{\zeta - 1} - 2\right)\frac{\partial\mu}{\partial x}\right], \\ v_r = \frac{\partial\Phi}{\partial r} &= -\frac{Ube}{E}\left[\mu\left(\ln\frac{\zeta + 1}{\zeta - 1} - \frac{2\zeta}{\zeta^2 - 1}\right)\frac{\partial\zeta}{\partial r} + \left(\zeta \ln\frac{\zeta + 1}{\zeta - 1} - 2\right)\frac{\partial\mu}{\partial r}\right]. \end{aligned}\right\} \quad (A.6)$$

The partial derivatives of ζ and μ with respect to x and r are determined by differentiating the system (A.2) partially, while considering first r and then x as constants:

$$\left.\begin{aligned} \frac{\partial\zeta}{\partial x} &= \frac{\mu(\zeta^2-1)}{be(\zeta^2-\mu^2)} \quad ; \qquad \frac{\partial\mu}{\partial x} = \frac{\zeta(1-\mu^2)}{be(\zeta^2-\mu^2)} \quad ; \\ \frac{\partial\zeta}{\partial r} &= \frac{r\zeta}{b^2e^2(\zeta^2-\mu^2)} \quad ; \qquad \frac{\partial\mu}{\partial r} = -\frac{r\mu}{b^2e^2(\zeta^2-\mu^2)} \, . \end{aligned}\right\} \quad \ldots \quad \ldots \quad \ldots \quad \text{(A.7)}$$

Introducing (A.7) into (A.6) and simplifying, we get:

$$\left.\begin{aligned} -E\frac{v_x}{U} &= \ln\frac{\zeta+1}{\zeta-1} - \frac{2\zeta}{\zeta^2-\mu^2} \, , \\ E\frac{v_r}{U} &= \frac{2\mu}{\zeta^2-\mu^2}\left(\frac{1-\mu^2}{\zeta^2-1}\right)^{1/2} . \end{aligned}\right\} \quad \ldots \quad \ldots \quad \ldots \quad \ldots \quad \ldots \quad \text{(A.8)}$$

The velocity components *on the surface of the given ellipsoid* (corresponding to ' induced velocity components ' of section 2) are now found by substituting:

$$\zeta = \zeta_0 = 1/e \, , \quad \ldots \quad \ldots \quad \ldots \quad \ldots \quad \ldots \quad \ldots \quad \ldots \quad \ldots \quad \text{(A.9)}$$

and hence from the first of equations (A.2):

$$\mu = x/b = \xi \, , \quad \ldots \quad \ldots \quad \ldots \quad \ldots \quad \ldots \quad \ldots \quad \ldots \quad \ldots \quad \text{(A.10)}$$

whereupon (A.8) yield:

$$-\frac{v_x}{U} = \frac{1}{E}\left(\ln\frac{1+e}{1-e} - \frac{2e}{1-e^2\xi^2}\right), \quad \ldots \quad \ldots \quad \ldots \quad \ldots \quad \ldots \quad \ldots \quad \text{(A.11)}$$

$$\frac{v_r}{U} = \frac{2e^3\xi(1-\xi^2)^{1/2}}{E(1-e^2)^{1/2}(1-e^2\xi^2)} \, . \quad \ldots \quad \ldots \quad \ldots \quad \ldots \quad \ldots \quad \ldots \quad \text{(A.12)}$$

When considering a steady flow of the air, with velocity $(-U)$ at infinity, past the fixed ellipsoid, v_r remains as given by (A.12), while the axial component becomes $(-U+v_x)$, expressed according to (A.11) and (A.5):

$$\frac{-U+v_x}{U} = -\frac{2e^3(1-\xi^2)}{E(1-e^2)(1-e^2\xi^2)} \, . \quad \ldots \quad \ldots \quad \ldots \quad \ldots \quad \ldots \quad \ldots \quad \text{(A.13)}$$

The resultant velocity V and its angle α with the x axis will now be given by:

$$\frac{V}{U} = \frac{\{(-U+v_x)^2+v_r^2\}^{1/2}}{U} = \frac{2e^3}{E(1-e^2)}\left(\frac{1-\xi^2}{1-e^2\xi^2}\right)^{1/2} \ldots \quad \ldots \quad \ldots \quad \text{(A.14)}$$

and

$$\tan\alpha = \frac{v_r}{-U+v_x} = -\frac{(1-e^2)^{1/2}\cdot\xi}{(1-\xi^2)^{1/2}} = -\frac{\vartheta\xi}{(1-\xi^2)^{1/2}} \, . \ldots \quad \ldots \quad \ldots \quad \text{(A.15)}$$

The latter formula shows that the *boundary conditions are exactly satisfied*, and the former leads to the *exact supervelocity ratio :*

$$\frac{\Delta V}{U} = \frac{V-U}{U} = \frac{2e^3}{E(1-e^2)}\left(\frac{1-\xi^2}{1-e^2\xi^2}\right)^{1/2} - 1 \quad \ldots \quad \ldots \quad \ldots \quad \ldots \quad \text{(A.16)}$$

In Fig. 16, the graphs of (A.11) and (A.16) are traced as full curves, with E given by (A.5), for the thickness ratio $\vartheta = 0{\cdot}16$ and corresponding $e = 0{\cdot}987117$. The approximate curves from Figs. 3 and 3a, as calculated before from (4.2.3) and (4.2.4) are also shown (broken lines), and it is seen that the agreement is very satisfactory, in view of the large scale of ordinates. It may be

noticed that, at the nose ($\xi = 1$), the formula (A.11) gives $v_x/U = 1$, while (4.2.3) would lead to $v_x/U = \infty$, but this discrepancy must always occur at stagnation points and is practically unimportant. The *point where* $v_x = 0$ is obtained from (A.11) at

$$(\xi)_{v_x = 0} = \frac{1}{e}\left(1 - \frac{2e}{\ln \frac{1+e}{1-e}}\right)^{1/2}, \quad \ldots \quad \ldots \quad \ldots \quad \ldots \quad \ldots \quad \ldots \quad \text{(A.17)}$$

and from (4.2.3):

$$(\xi)_{v_x = 0} \simeq \left(1 - \frac{1}{\ln \frac{2}{\vartheta}}\right)^{1/2}, \quad \ldots \quad \ldots \quad \ldots \quad \ldots \quad \ldots \quad \ldots \quad \ldots \quad \text{(A.18)}$$

the two values in the given case being 0·790 and 0·777, respectively (Fig. 16, left-hand side). The *point of zero resultant supervelocity* ($\Delta V = 0$) is similarly obtained from (A.16):

$$(\xi)_{\Delta V = 0} = \left(\frac{N^2 - 1}{N^2 - e^2}\right)^{1/2}, \quad \text{where} \quad N = \frac{2e^3}{E(1 - e^2)}, \quad \ldots \quad \ldots \quad \ldots \quad \ldots \quad \text{(A.19)}$$

and approximately, from (4.2.3) and (4.2.4) combined:

$$(\xi)_{\Delta V = 0} \simeq \left(\frac{2 \ln 2/\vartheta - 2}{2 \ln 2/\vartheta - 1}\right)^{1/2}, \quad \ldots \quad \ldots \quad \ldots \quad \ldots \quad \ldots \quad \ldots \quad \ldots \quad \text{(A.20)}$$

and the numerical values in the given case are 0·879 and 0·868 (Fig. 16, right-hand side).

The *exact maximum supervelocity ratio* from (A.11) or (A.16) is:

$$\delta = \left(-\frac{v_x}{U}\right)_{\max} = \left(\frac{\Delta V}{U}\right)_{\max} = \frac{\ln \frac{1+e}{1-e} - 2e}{\frac{2e}{1-e^2} - \ln \frac{1+e}{1-e}}, \quad \ldots \quad \ldots \quad \ldots \quad \text{(A.21)}$$

becoming 0 for $e \to 1$, and 1/2 for $e \to 0$ (sphere), *see* Ref. 14, while the approximate expression has been found as (4.2.5). For $\vartheta = 0{\cdot}16$ the two values are 0·0425 and 0·0391, respectively. In Fig. 17, two curves represent δ for varying ϑ, from (A.21) and (4.2.5) respectively. It is seen that the agreement is generally satisfactory, but it deteriorates with increasing ϑ, as it had to be expected. In practice the method will hardly be used for ϑ exceeding 0·2, but even for thicker bodies the approximate velocity distribution should be at least qualitatively correct although numerically less accurate. The approximate numerical values will normally under-estimate the supervelocity slightly.

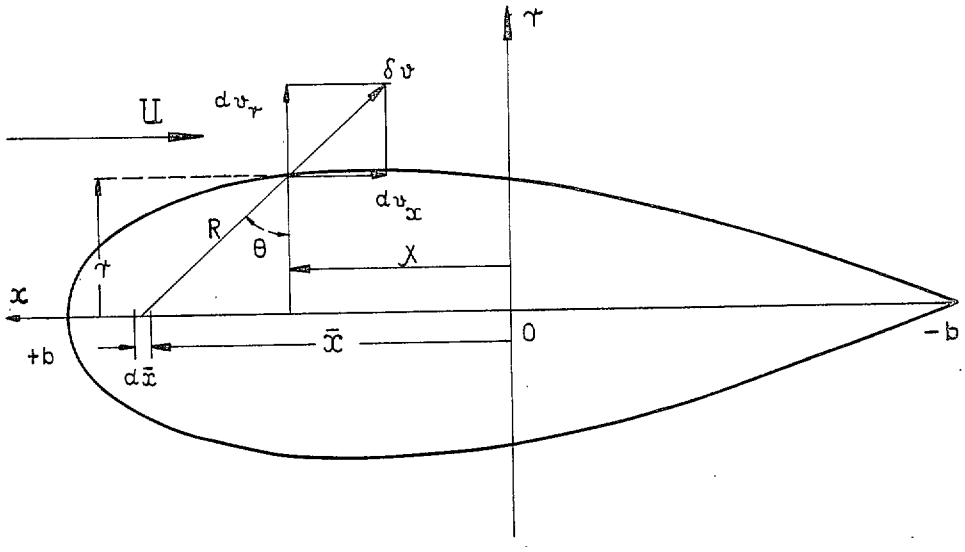

FIG. 1. Infinitesimal velocity components induced on the body surface by a source element.

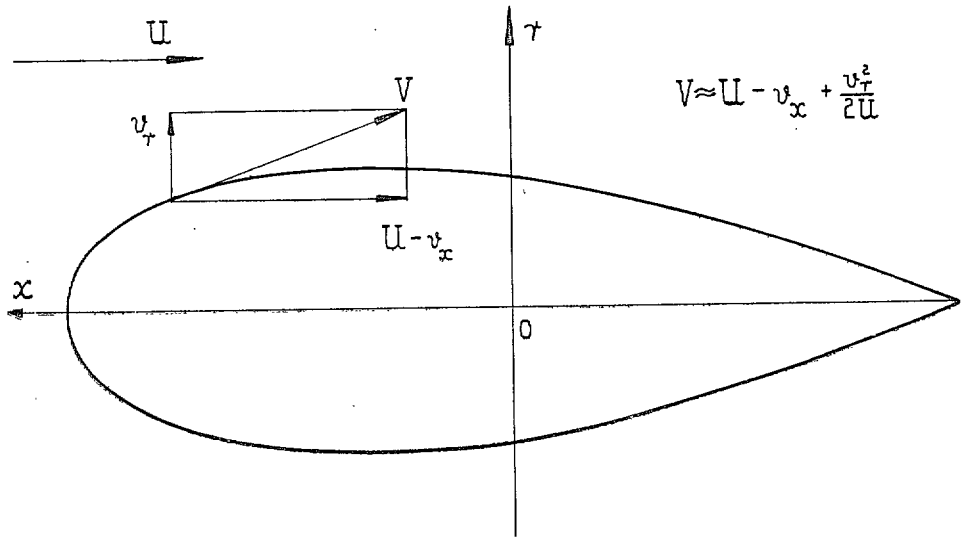

FIG. 2. Resultant induced velocities on the body surface.

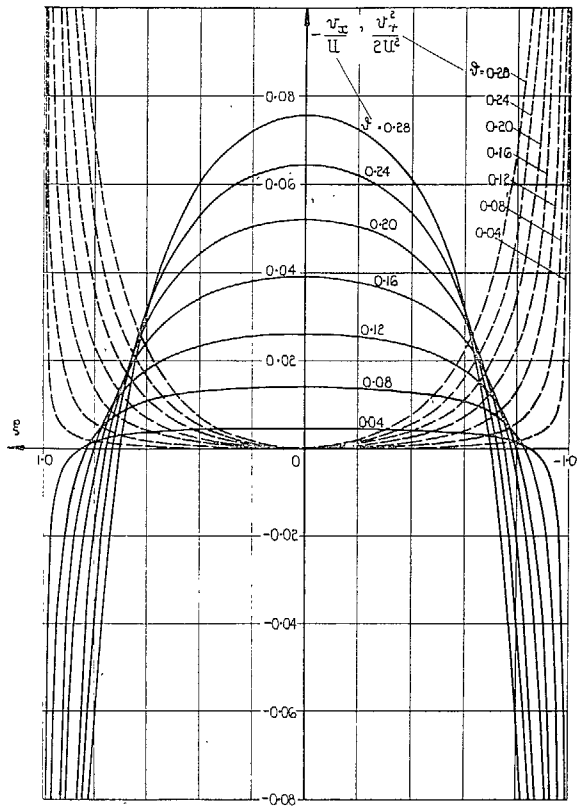

FIG.3

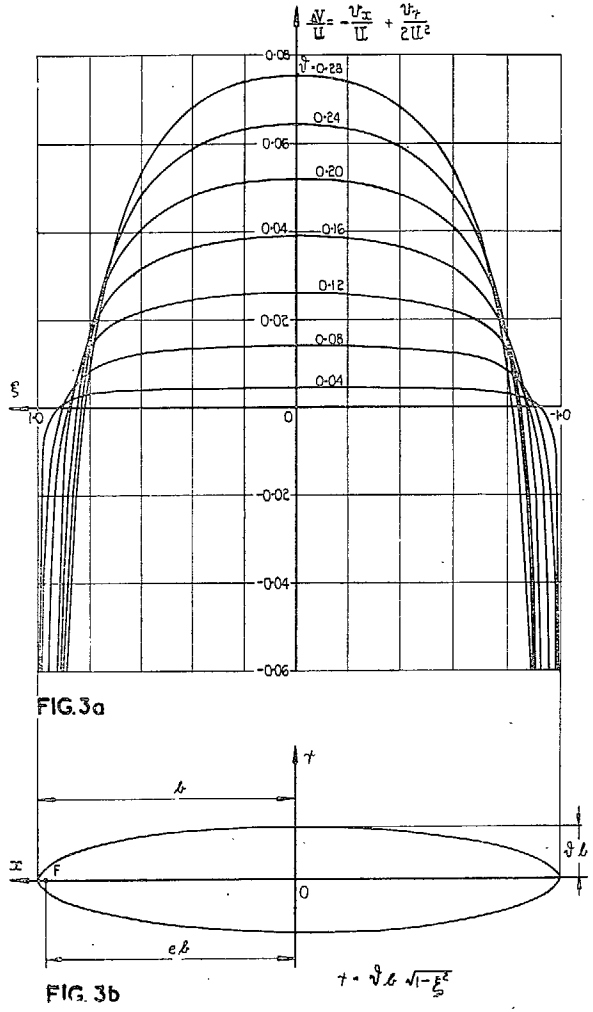

FIG.3a

FIG. 3b

FIGS. 3, 3a and 3b. Induced velocity components and resultant supervelocities for elongated ellipsoids of revolution.

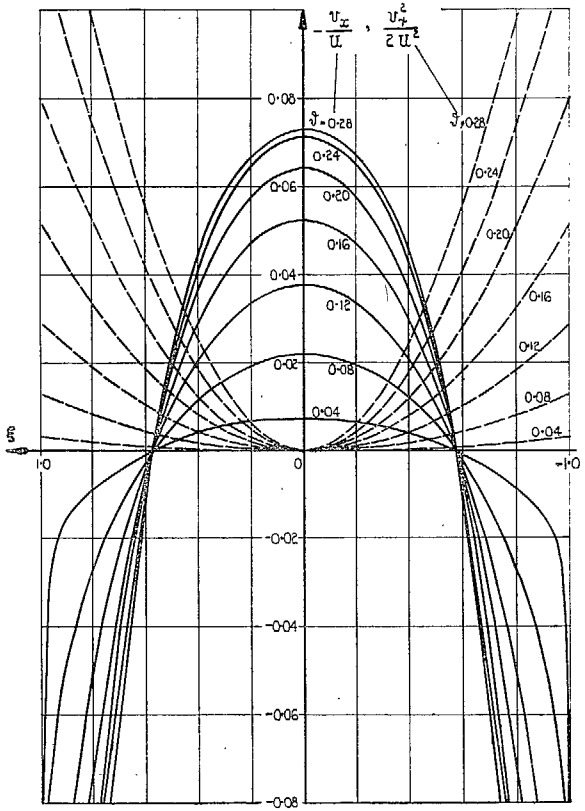

FIG. 4

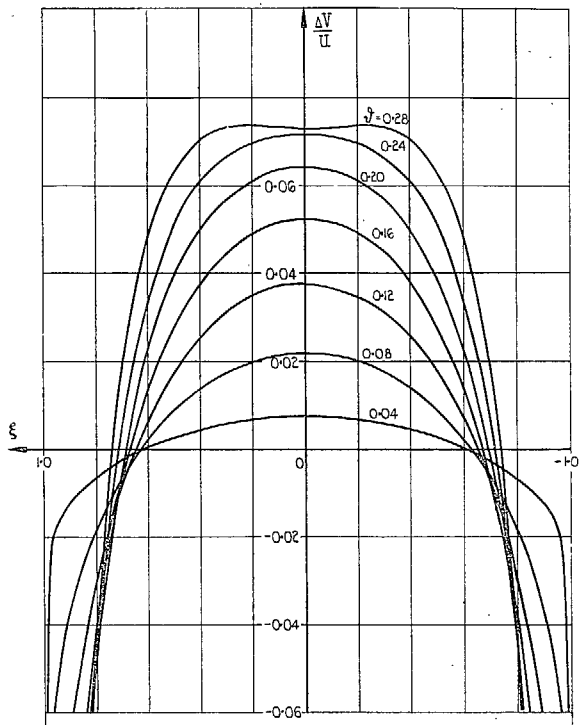

FIG. 4 a

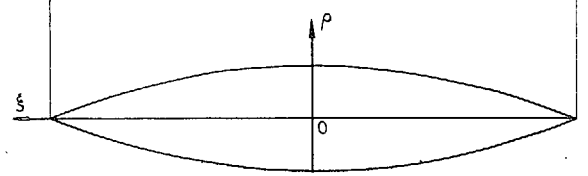

FIG. 4 b

FIGS. 4, 4a and 4b. Induced velocity components and resultant supervelocities for simple symmetrical bodies with pointed nose and tail end (parabolic meridian).

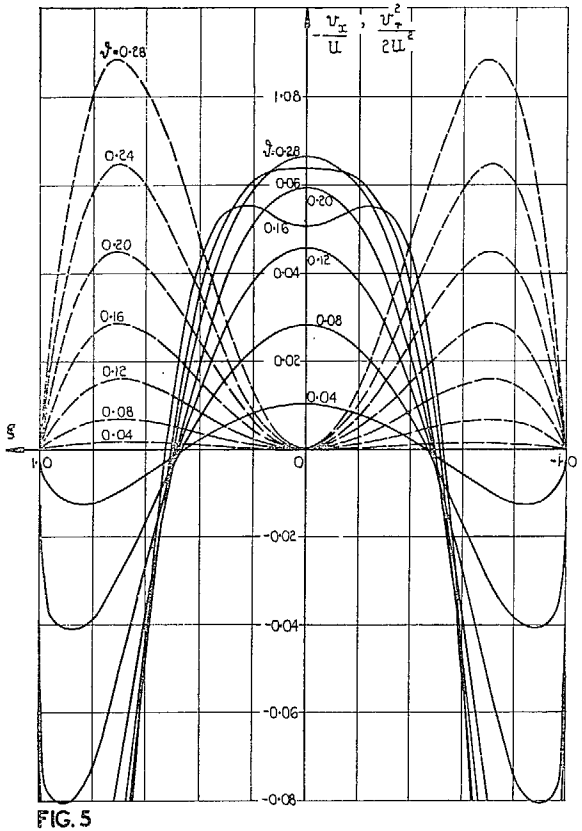

FIG. 5

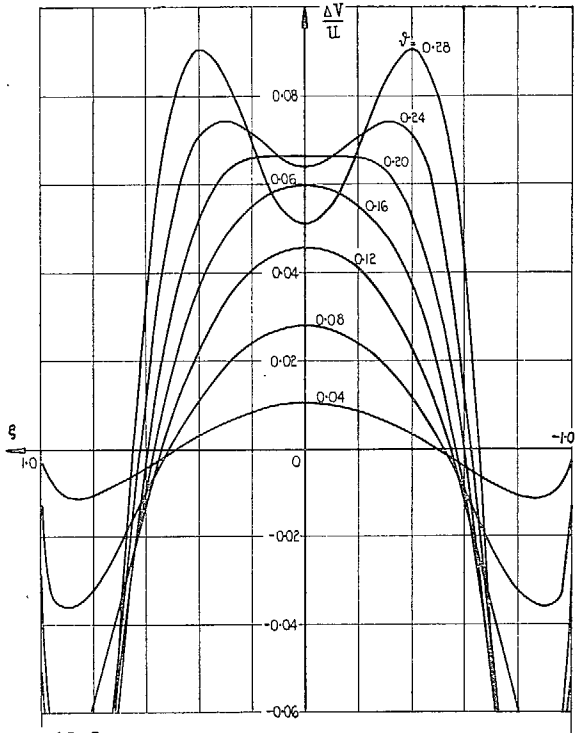

FIG. 5 a

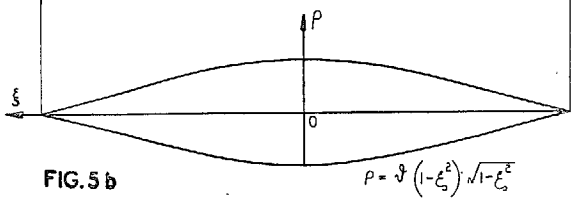

FIG. 5 b

FIGS. 5, 5a and 5b. Induced velocity components and supervelocities for simple symmetrical bodies with cusped nose and tail end.

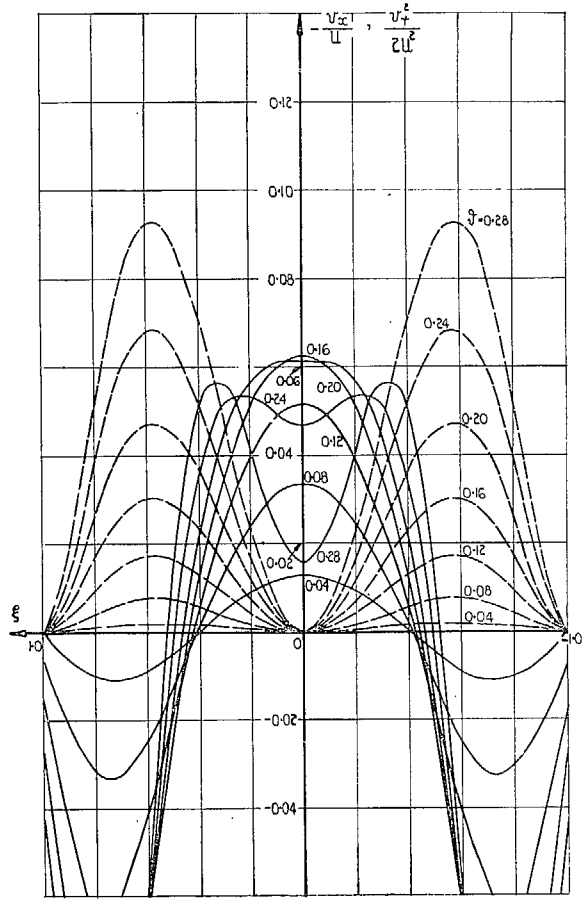

FIG. 6

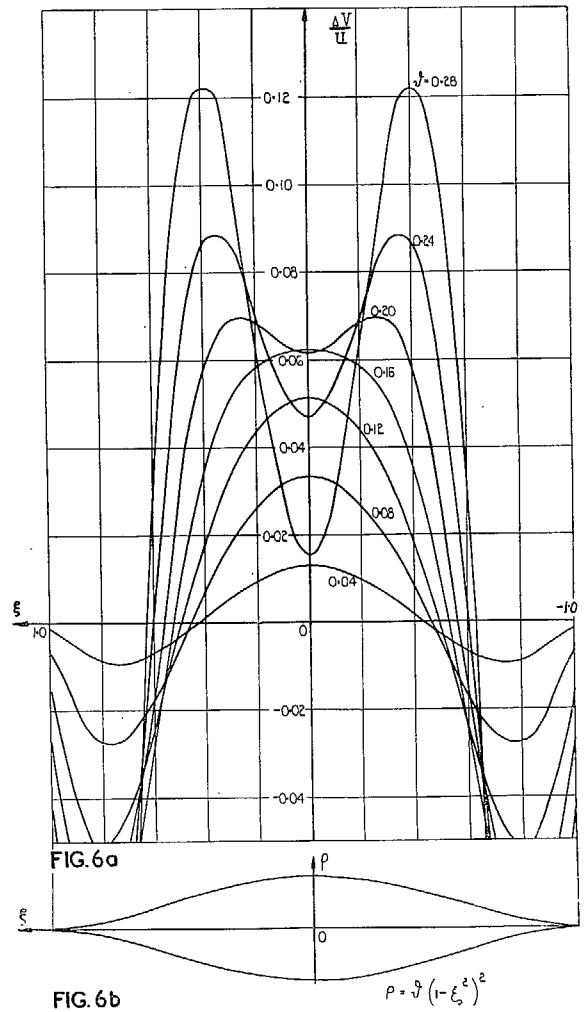

FIG. 6a

FIG. 6b

FIGS. 6, 6a and 6b. Induced velocity components and resultant supervelocities for simple symmetrical bodies with strongly cusped nose and tail end.

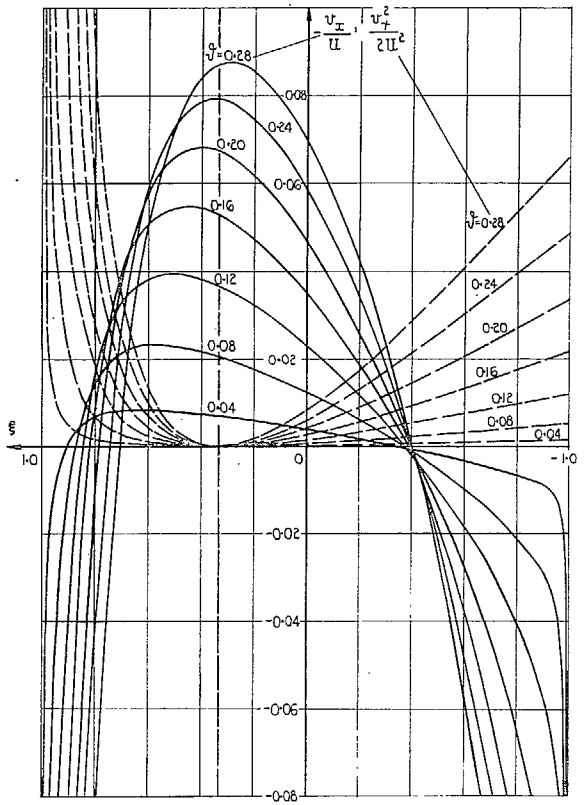

FIG.7

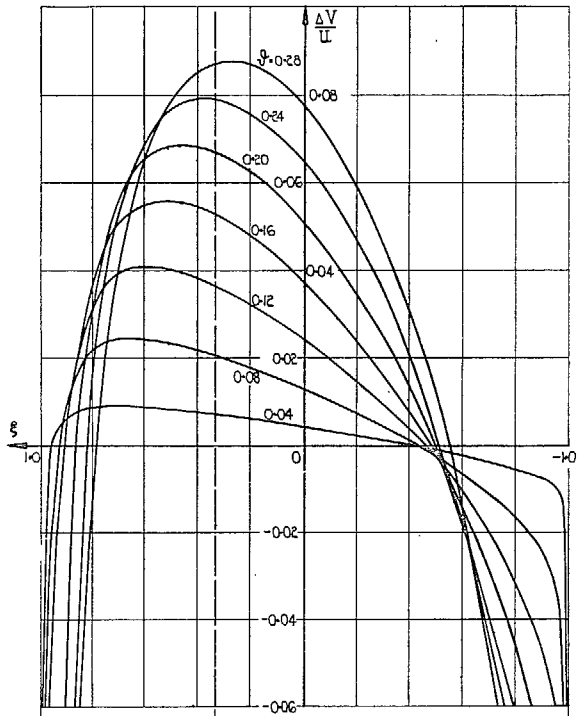

FIG.7a

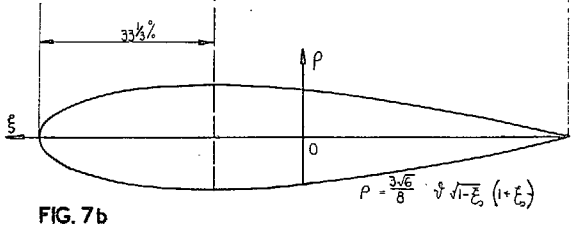

FIG. 7b

FIGS. 7, 7a and 7b. Induced velocity components and resultant supervelocities for simplest bodies with rounded nose and pointed tail end, maximum thickness at $33\frac{1}{3}$ per cent.

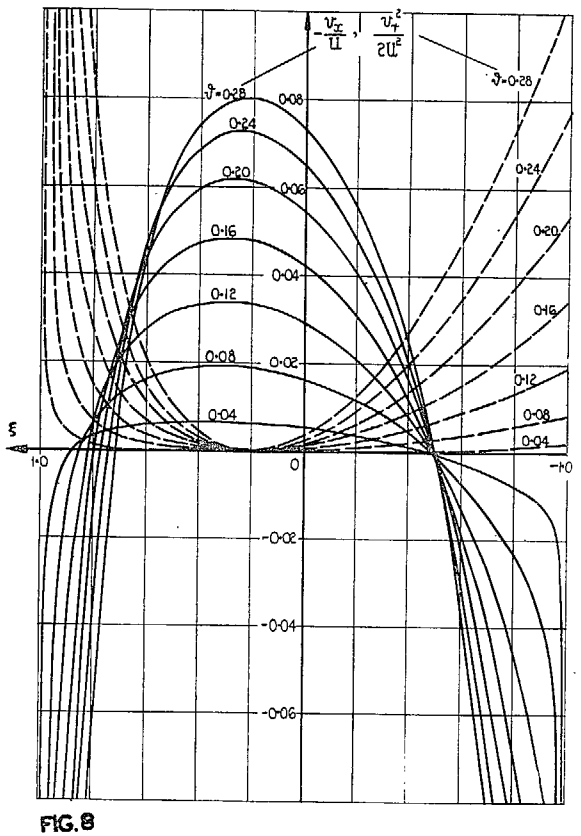

FIG. 8

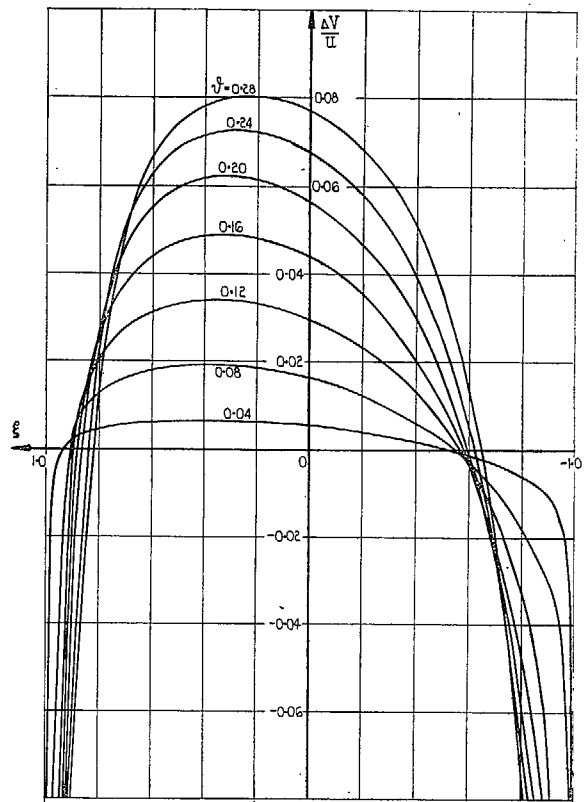

FIG. 8a

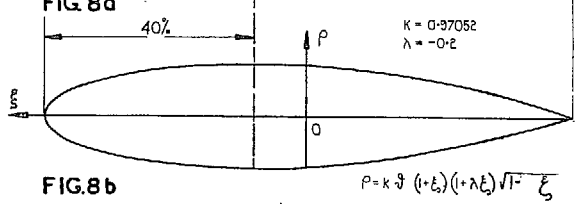

FIG. 8b

FIGS. 8, 8a and 8b. Induced velocity components and resultant supervelocities for simple bodies with rounded nose and pointed tail end, maximum thickness at 40 per cent.

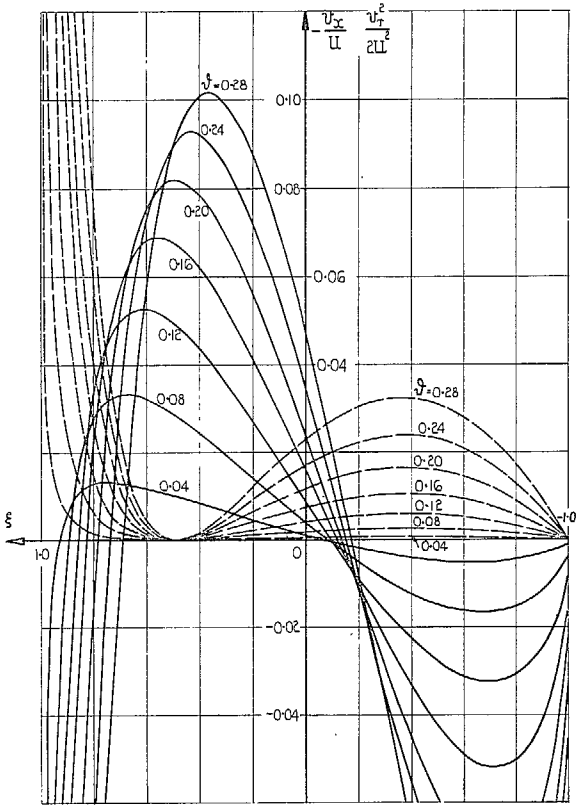

FIG. 9

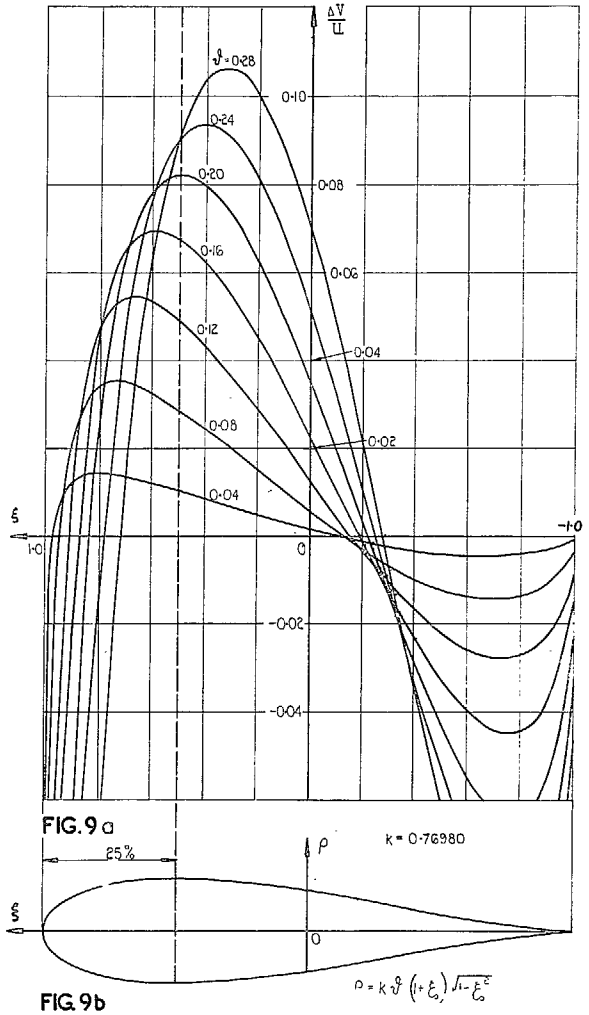

FIG. 9b

FIGS. 9, 9a and 9b. Induced velocity components and resultant supervelocities for simple bodies with rounded nose and cusped tail end, maximum thickness at 25 per cent.

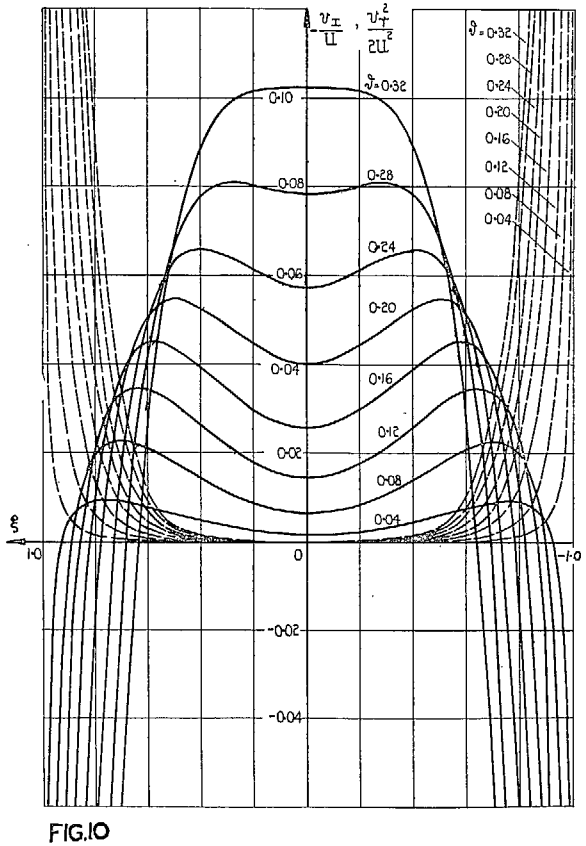

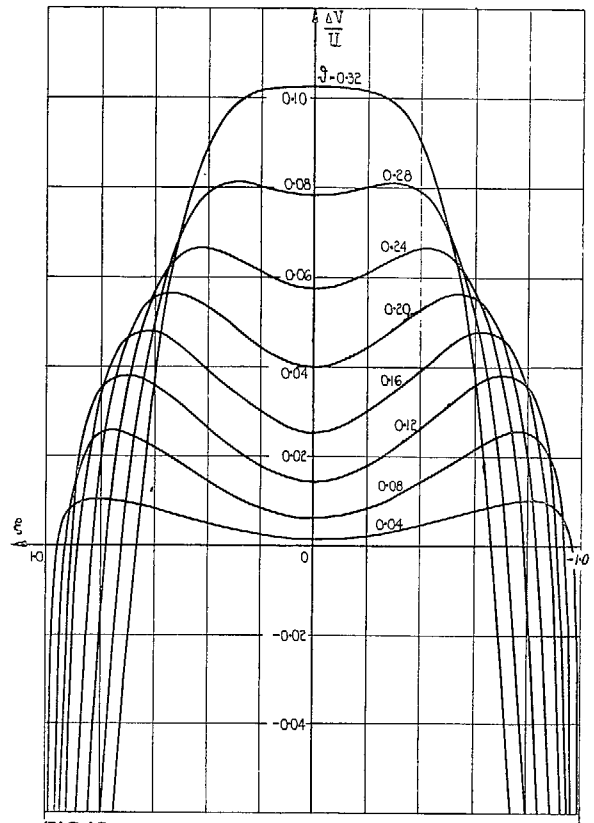

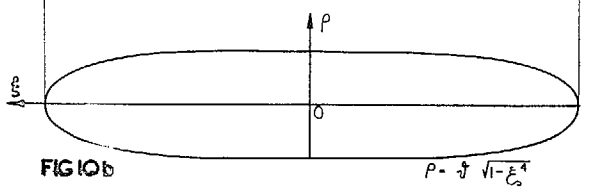

FIGS. 10, 10a and 10b. Induced velocity components and resultant supervelocities for nearly cylindrical symmetrical bodies with rounded nose and tail end.

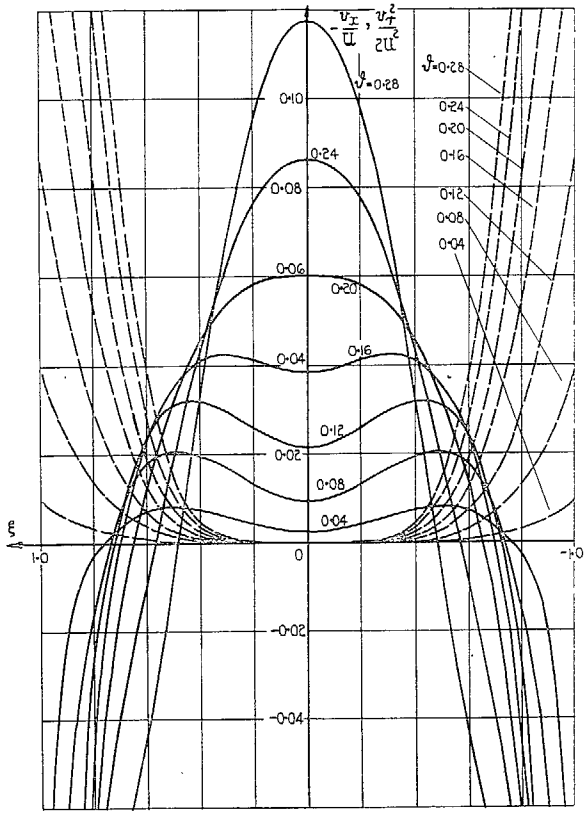

FIG. 11

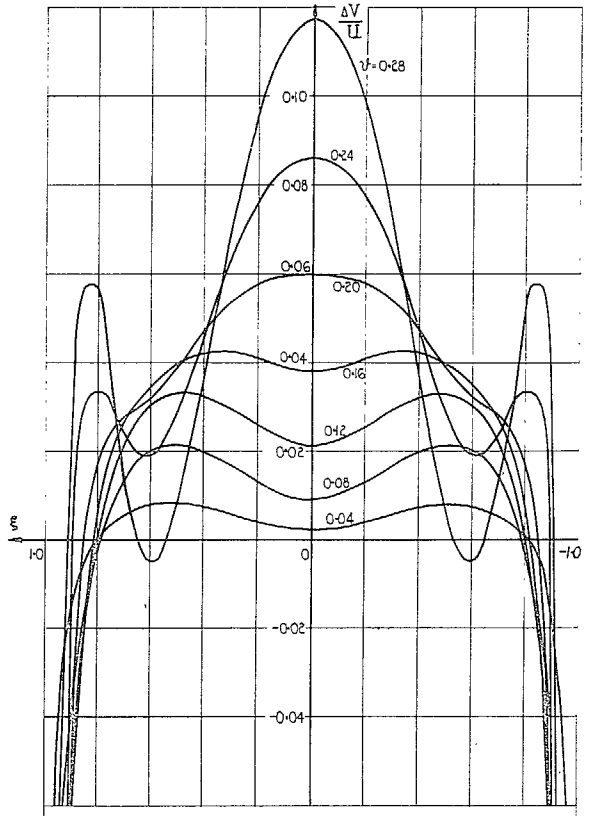

FIG. 11a

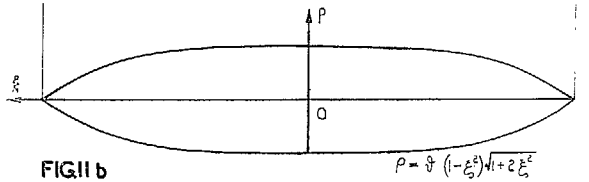

FIG. 11b

FIGS. 11, 11a and 11b. Induced velocity components and resultant supervelocities for nearly cylindrical bodies with pointed nose and tail end.

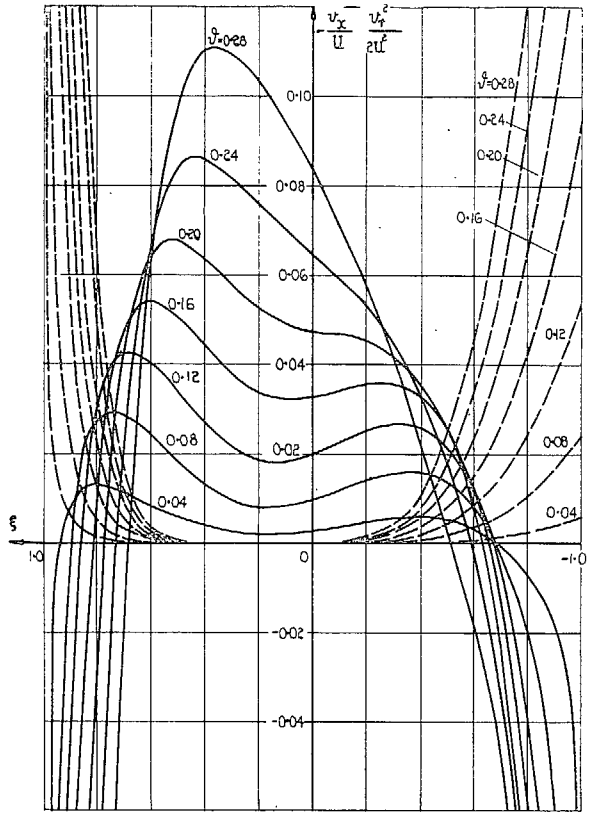

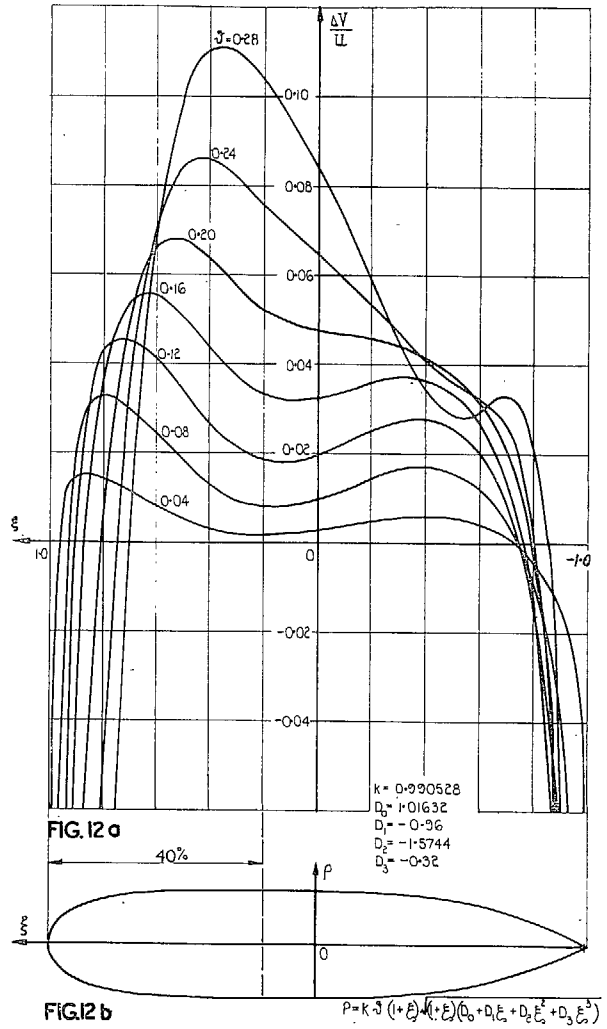

FIGS. 12, 12a and 12b. Induced velocity components and resultant supervelocities for nearly cylindrical bodies with rounded nose and pointed tail end, maximum thickness at 40 per cent.

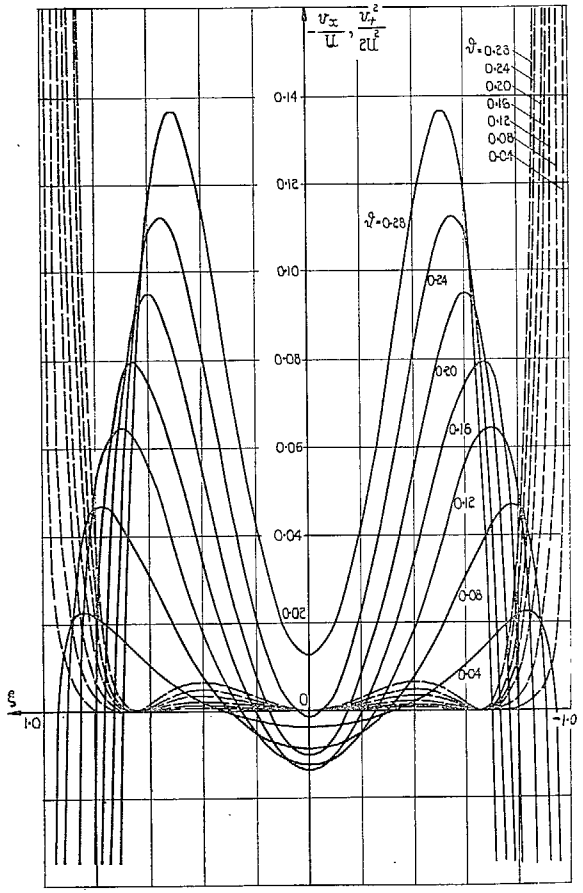

FIG.13

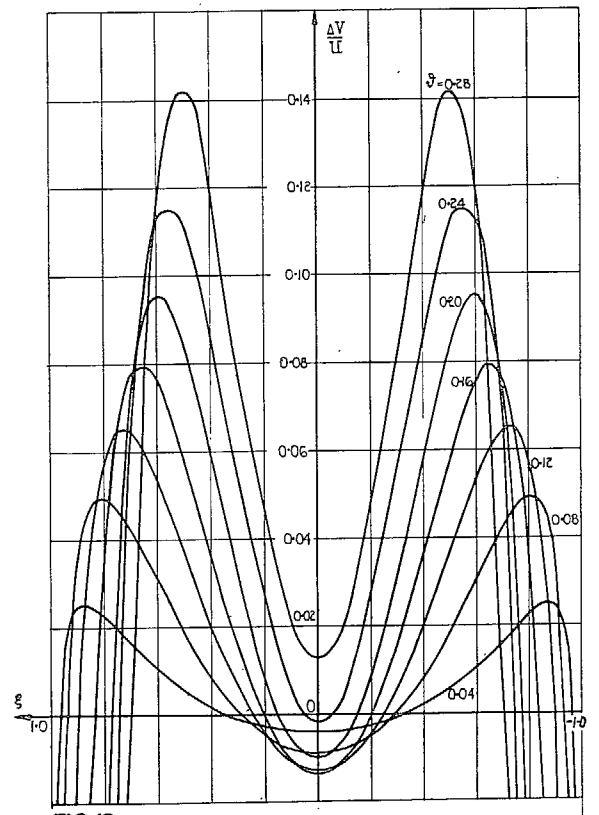

FIG. 13a

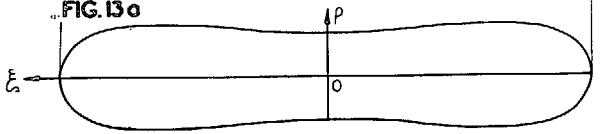

FIG. 13b

$\rho = k\vartheta\sqrt{1-\xi^2}\,(1+\nu\,\xi^2)$
μ = 1·4 k = 0·826797

FIGS. 13, 13a and 13b. Induced velocity components and resultant supervelocities for symmetrical bodies with central waist and rounded nose and tail end.

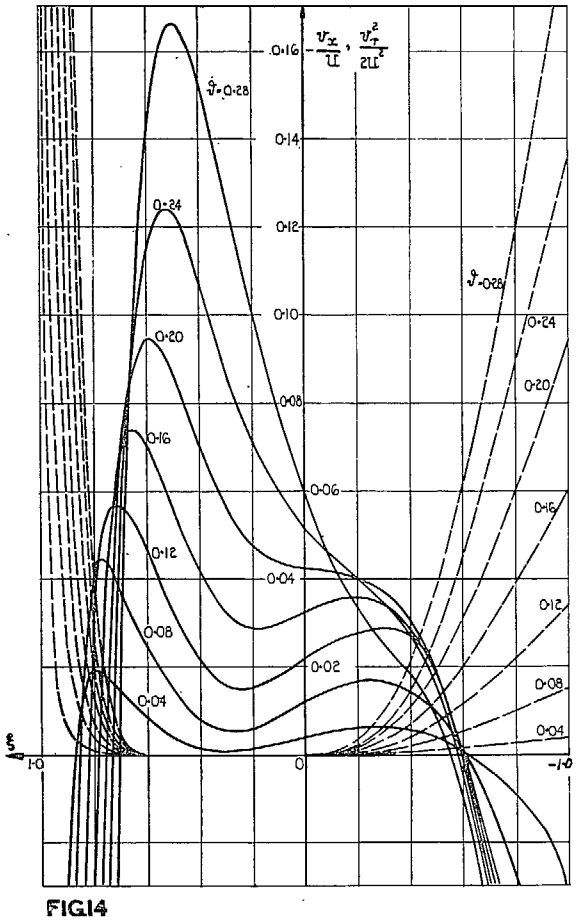

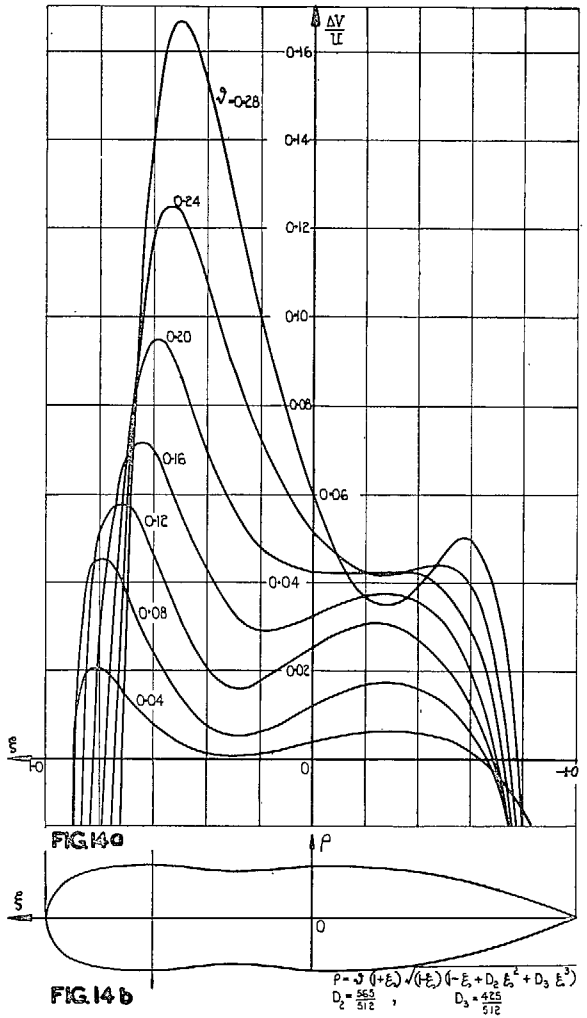

FIGS. 14, 14a and 14b. Induced velocity components and resultant supervelocities for bodies with rounded nose, pointed tail and a shallow waist.

(57670) Wt. 17/980 K.9 12/53 Hw.

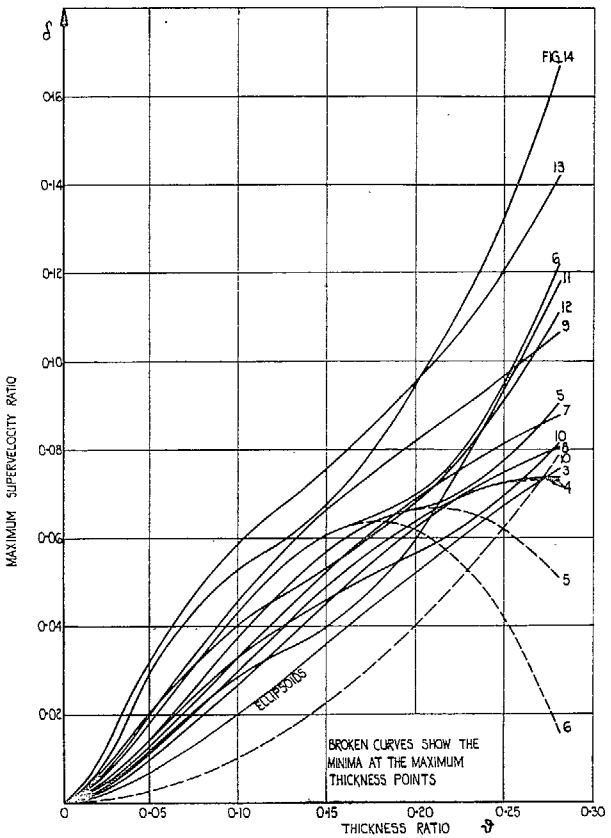

FIG. 15. Maximum supervelocity ratio at varying thickness ratio for twelve different bodies from Figs. 3–14.

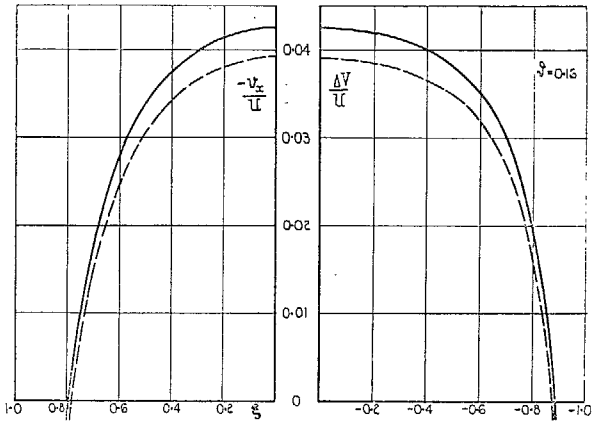

FIG. 16. Supervelocities on ellipsoid from exact and approximate methods.

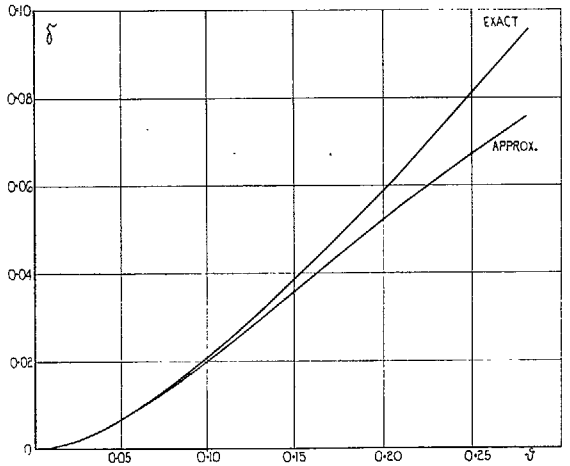

FIG. 17. Maximum supervelocity ratio for ellipsoids of varying thickness ratio, from exact and approximate methods.

PRINTED IN GREAT BRITAIN

Publications of the Aeronautical Research Council

ANNUAL TECHNICAL REPORTS OF THE AERONAUTICAL RESEARCH COUNCIL (BOUND VOLUMES)

1936 Vol. I. Aerodynamics General, Performance, Airscrews, Flutter and Spinning. 40*s.* (40*s.* 9*d.*)
Vol. II. Stability and Control, Structures, Seaplanes, Engines, etc. 50*s.* (50*s.* 10*d.*)

1937 Vol. I. Aerodynamics General, Performance, Airscrews, Flutter and Spinning. 40*s.* (40*s.* 10*d.*)
Vol. II. Stability and Control, Structures, Seaplanes, Engines, etc. 60*s.* (61*s.*)

1938 Vol. I. Aerodynamics General, Performance, Airscrews. 50*s.* (51*s.*)
Vol. II. Stability and Control, Flutter, Structures, Seaplanes, Wind Tunnels, Materials. 30*s.* (30*s.* 9*d.*)

1939 Vol. I. Aerodynamics General, Performance, Airscrews, Engines. 50*s.* (50*s.* 11*d.*)
Vol. II. Stability and Control, Flutter and Vibration, Instruments, Structures, Seaplanes, etc. 63*s.* (64*s.* 2*d.*)

1940 Aero and Hydrodynamics, Aerofoils, Airscrews, Engines, Flutter, Icing, Stability and Control, Structures, and a miscellaneous section. 50*s.* (51*s.*)

1941 Aero and Hydrodynamics, Aerofoils, Airscrews, Engines, Flutter, Stability and Control, Structures. 63*s.* (64*s.* 2*d.*)

1942 Vol. I. Aero and Hydrodynamics, Aerofoils, Airscrews, Engines. 75*s.* (76*s.* 3*d.*)
Vol. II. Noise, Parachutes, Stability and Control, Structures, Vibration, Wind Tunnels. 47*s.* 6*d.* (48*s.* 5*d.*)

1943 Vol. I. (*In the press.*)
Vol. II. (*In the press.*)

ANNUAL REPORTS OF THE AERONAUTICAL RESEARCH COUNCIL—

1933–34	1*s.* 6*d.* (1*s.* 8*d.*)	1937	2*s.* (2*s.* 2*d.*)
1934–35	1*s.* 6*d.* (1*s.* 8*d.*)	1938	1*s.* 6*d.* (1*s.* 8*d.*)
April 1, 1935 to Dec. 31, 1936.	4*s.* (4*s.* 4*d.*)	1939–48	3*s.* (3*s.* 2*d.*)

INDEX TO ALL REPORTS AND MEMORANDA PUBLISHED IN THE ANNUAL TECHNICAL REPORTS, AND SEPARATELY—

April, 1950 - - - - R. & M. No. 2600. 2*s.* 6*d.* (2*s.* 7½*d.*)

AUTHOR INDEX TO ALL REPORTS AND MEMORANDA OF THE AERONAUTICAL RESEARCH COUNCIL—

1909–1949. R. & M. No. 2570. 15*s.* (15*s.* 3*d.*)

INDEXES TO THE TECHNICAL REPORTS OF THE AERONAUTICAL RESEARCH COUNCIL—

December 1, 1936 — June 30, 1939.	R. & M. No. 1850.	1*s.* 3*d.* (1*s.* 4½*d.*)
July 1, 1939 — June 30, 1945.	R. & M. No. 1950.	1*s.* (1*s.* 1½*d.*)
July 1, 1945 — June 30, 1946.	R. & M. No. 2050.	1*s.* (1*s.* 1½*d.*)
July 1, 1946 — December 31, 1946.	R. & M. No. 2150.	1*s.* 3*d.* (1*s.* 4½*d.*)
January 1, 1947 — June 30, 1947.	R. & M. No. 2250.	1*s.* 3*d.* (1*s.* 4½*d.*)
July, 1951.	R. & M. No. 2350.	1*s.* 9*d.* (1*s.* 10½*d.*)

Prices in brackets include postage.

Obtainable from

HER MAJESTY'S STATIONERY OFFICE

York House, Kingsway, London, W.C.2; 423 Oxford Street, London, W.1 (Post Orders: P.O. Box 569, London, S.E.1); 13a Castle Street, Edinburgh 2; 39, King Street, Manchester, 2; 2 Edmund Street, Birmingham 3; 1 St. Andrew's Crescent, Cardiff; Tower Lane, Bristol 1; 80 Chichester Street, Belfast, or through any bookseller

S.O. Code No. 23-2814